

DISCONTINUITY INDUCED HOPF AND NEIMARK-SACKER BIFURCATIONS IN A MEMRISTIVE MURALI-LAKSHMANAN-CHUA CIRCUIT

A. ISHAQ AHAMED

*Department of Physics, Jamal Mohamed College,
Tiruchirappalli-620020, India
ishaq1970@gmail.com*

M. LAKSHMANAN

*Centre for Nonlinear Dynamics, School of Physics,
Bharathidasan University,
Tiruchirappalli-620024, India
lakshman@gmail.com*

Received (to be inserted by publisher)

We report using Clarke's concept of generalised differential and a modification of Floquet theory to non-smooth oscillations, the occurrence of discontinuity induced Hopf bifurcations and Neimark-Sacker bifurcations leading to quasiperiodic attractors in a memristive Murali-Lakshmanan-Chua (memristive MLC) circuit. The above bifurcations arise because of the fact that a memristive MLC circuit is basically a nonsmooth system by virtue of having a memristive element as its nonlinearity. The switching and modulating properties of the memristor which we have considered endow the circuit with two discontinuity boundaries and multiple equilibrium points as well. As the Jacobian matrices about these equilibrium points are non-invertible, they are non-hyperbolic, some of these admit local bifurcations as well. Consequently when these equilibrium points are perturbed, they lose their stability giving rise to quasiperiodic orbits. The numerical simulations carried out by incorporating proper discontinuity mappings (DMs), such as the Poincaré discontinuity map (PDM) and zero time discontinuity map (ZDM), are found to agree well with experimental observations.

Keywords: memristive MLC circuit, non-hyperbolicity, switching manifolds, discontinuity induced bifurcations, Clarke's generalised differential, Hopf bifurcations and Neimark-Sacker bifurcations

1. Introduction

A memristor can be defined as any two-terminal device which exhibits a pinched hysteresis loop in the $(v - i)$ plane when driven by a bipolar periodic voltage or current excitation waveform, for any initial conditions [Chua, 2014]. Its existence was first postulated by Leon O. Chua in the year 1971, purely from theoretical arguments [Chua, 1971]. Almost four decades later, Strukov et al. of Hewlett-Packard Laboratories designed the first approximate physical example of a memristor [Strukov *et al.*, 2008] in a solid-state nano-scale system in which electronic and ionic transports are coupled under an external bias

voltage. Immediately following this announcement, a theoretical study of memristive oscillators was made by Itoh & Chua [2008], which initiated a new field of research in memristive oscillators.

The $(v - i)$ characteristic of memristors is inherently non-linear [Chua, 1971], because of which it is endowed with many peculiar features such as resistive switching at extremely high two-terminal device densities [Tour & He, 2008], pinched hysteresis characteristic and modulating ability [Ishaq Ahamed *et al.*, 2011]. As a result of these, the memristor is considered as a desirable element in many circuit applications. For example, memristor based chaotic circuits and their implementations were described in references [Muthuswamy, 2009; Muthuswamy & Kokate, 2009; Muthuswamy, 2010; Muthuswamy & Chua, 2010]. The existence of chaotic beats in a memristive Chua's circuit was reported in Ishaq Ahamed *et al.* [2011] and hyperchaotic beats, hyperchaos and transient hyperchaos in a memristive Murali-Lakshmanan-Chua (MLC) circuit by Ishaq & Lakshmanan [2013]. The coexistence of infinitely many stable periodic orbits and stable equilibrium points has been reported in memristive oscillators by Messias *et al.* [2010]. Chaos and its control in a four dimensional memristor based circuit using a twin-T Notch filter have been studied in [Iu *et al.*, 2011]. Transient chaos has also been reported in a memristive canonical Chua's circuit by [Bo-Cheng *et al.*, 2010; Bao *et al.*, 2010]. The dynamical behaviour and stability analysis of a fractional-order memristor based Chua's circuit were investigated by Petráš [2010]. The nonlinear dynamics of a network of memristor oscillators was investigated by Corinto & Gilli [2011]. Memristive chaotic circuits based on cellular nonlinear networks were studied by Buscarino *et al.* [2012].

In our earlier works on memristive circuits, we had identified the memristive Chua's circuit and memristive MLC circuit as non-smooth systems by virtue of the inclusion of a memristor as their nonlinear element. In particular, we identified that the primary cause of hyper-chaos, transient hyper-chaos and hyperchaotic beats that arose in memristive MLC circuit was the occurrence of *grazing bifurcations*- a type of discontinuity induced bifurcation. But many other types of discontinuity bifurcations were found to arise in non-smooth systems, namely *sliding bifurcations*, such as *crossing-sliding*, *switching-sliding*, *grazing-sliding* and *adding-sliding* bifurcations. In addition many other bifurcations such as *impact oscillations* in a bouncing ball [Babitskii, 1978; Feigin, 1994], *stick-slip* oscillations in mechanical systems [Galvanaetto, 1997, 2001; Galvanaetto & Bishop, 1998; Babitskii, 1978] were reported. Further *discontinuity induced Hopf bifurcations* leading to *limit cycle oscillations* were reported in non-smooth planar systems by Leine & Campen [2006] and in the Chua's oscillator in two separate works by Zhang & Bi [2012] and Fu *et al.* [2015]. Hence naturally a question arose as to the other types of bifurcations that may arise in the simple memristive MLC circuit. Our consequent works on the memristive MLC circuit led us to the identification of discontinuity induced *Hopf* bifurcations and discontinuity induced *secondary Hopf* or *Neimark-Sacker* bifurcations leading to quasiperiodic oscillations and different types of *sliding bifurcations*. In this paper we report the occurrence of discontinuity induced *Hopf* bifurcations and discontinuity induced *Neimark-Sackur* bifurcations in the memristive MLC circuit. The incidence of *sliding* bifurcations in the memristive MLC circuit will be reported in subsequent articles.

The paper is organised as follows. In Sec. 2, we discuss the peculiar features of a the flux controlled memristor such as resistive switching property and modulating ability. In Sec. 3, the memristive MLC circuit, its circuit equations and their normalized forms using proper rescaling parameters are given. In Sec. 4, the memristive MLC circuit is considered as a piecewise smooth continuous system. Its switching manifolds are identified and the system equations are reformulated as a set of smooth ODEs. The various equilibrium points admitted by this system are evaluated and their stability analysed. In Sec. 5, the memristive MLC circuit is considered for the unforced case, and the discontinuity induced Hopf bifurcation exhibited by it under such a condition is studied by numerical simulations using Clarke's generalised differentials and by hardware experiments. In Sec. 6, the scaling up of the amplitude of the oscillations under the action of an external forcing is described through numerics. In Sec. 7, the discontinuity induced Neimark-Sackur bifurcation admitted by the same system under the action of an external forcing is studied by using a modification of the Floquet theory to non-smooth oscillations. In Sec. 8, a consolidation of the work is presented.

2. Circuit Theoretic Properties: Resistive Switching and Memristive Modulation

In this section we give a brief introduction to the circuit theoretic properties of the memristor such as *resistive switching* and *memristive modulation* and how they naturally lead to quasiperiodicity in the memristive MLC circuit.

Generally a memristor is a two terminal device whose flux-linkage ϕ and charge q fall on some fixed curve in the $(q - \phi)$ plane and is represented mathematically as

$$g(\phi, q) = 0. \quad (1)$$

For a *flux controlled* memristor this relation is expressed as a single-valued function of flux-linkage ϕ . Consequently the constitutive relation becomes

$$i(t) = W(\phi)v(t), \quad (2)$$

where

$$W(\phi) = \frac{dq(\phi)}{d\phi}, \quad (3)$$

defines the incremental *memductance*. It is so called because it has the dimension of conductance, namely \mathcal{U} or Siemens.

The time varying resistive property of the resistors reported by Chua in [Chua *et al.*, 1987] can be easily extended to memristors. From Eq. (3) it is clear that the memductance $W(\phi)$ is a function of the flux-linkage ϕ . But from Faraday's law, the flux linkage is defined as the time integral of the voltage, namely

$$\phi(t) = \int_{-\infty}^t v(\tau)d\tau \quad (4)$$

Hence we can write

$$\begin{aligned} \phi(t) &= \int_{-\infty}^t v(\tau)d\tau \\ &= \int_{-\infty}^{t_0} v(\tau)d\tau + \int_{t_0}^t v(\tau)d\tau, \quad t \geq t_0 \\ &= \phi(t_0) + \int_{t_0}^t v(\tau)d\tau, \end{aligned} \quad (5)$$

where t_0 is some chosen value of t . If we assume $\phi(t_0) = 0$, then from the the above Eq. (5) the value of the flux-linkage ϕ at any instant of time t depends on the time integral of the voltage from some initial time t_0 to the instant of time t . Hence while a flux-controlled memristor behaves as an ordinary conductor at any given instant of time t , its total memductance depends on the complete past history of the memristor voltage.

These variations of the memductance as a function of time cause the memristor to possess both a time varying resistive property as well as a memory nature. As a result of these, the memristor is endowed with some desirable characteristic features such as *resistive switching property*, *modulating ability* etc., making it a desirable element in many circuit applications.

2.1. Resistive Switching

The resistive switching property of a memristor can be studied by using the analogy of an electrical switch. Let this switch be activated by sinusoidal variations of the flux(ϕ) having an angular frequency ω and a time period τ . When the flux exceeds a predetermined level, say B_p , let the switch be in ON state and when the flux falls below this level B_p let the switch be in OFF state. Mathematically this variation of the memductance can be represented as

$$W(t) = W(\phi(t)) = W(a) + W(b)\Phi(t), \quad (6)$$

where $W(a)$ and $W(b)$ are the parametric memductance values of the memristor and $\Phi(t)$ represents the Fourier series for an anti-symmetric square wave of amplitude Φ_m and frequency f_m .

$$\begin{aligned}\Phi(t) &= \frac{4\Phi_m}{\pi} \sum_{n=1}^{\infty} \frac{\sin((2n-1)2\pi f_m t)}{(2n-1)} \\ &= \frac{4\Phi_m}{\pi} \left\{ \sin(2\pi f_m t) + \frac{1}{3} \sin(6\pi f_m t) + \frac{1}{5} \sin(10\pi f_m t) + \dots \right\}.\end{aligned}\quad (7)$$

The variations in parametric memductance values causes the resultant memductance $W(\phi)$ of the memristor to vary as a function of time t , with a low OFF state value of $W_1 = W(a)$ and high ON state value of $W_2 = W(a) + W(b)$ $\left(\frac{4\Phi_m}{\pi} \sum_{n=1}^{\infty} \frac{\sin((2n-1)2\pi f_m t)}{(2n-1)} \right)$. These variations take place at a constant frequency f_m and define the resistive switching characteristic of the memristor with time t , as shown in Fig. 1(a).

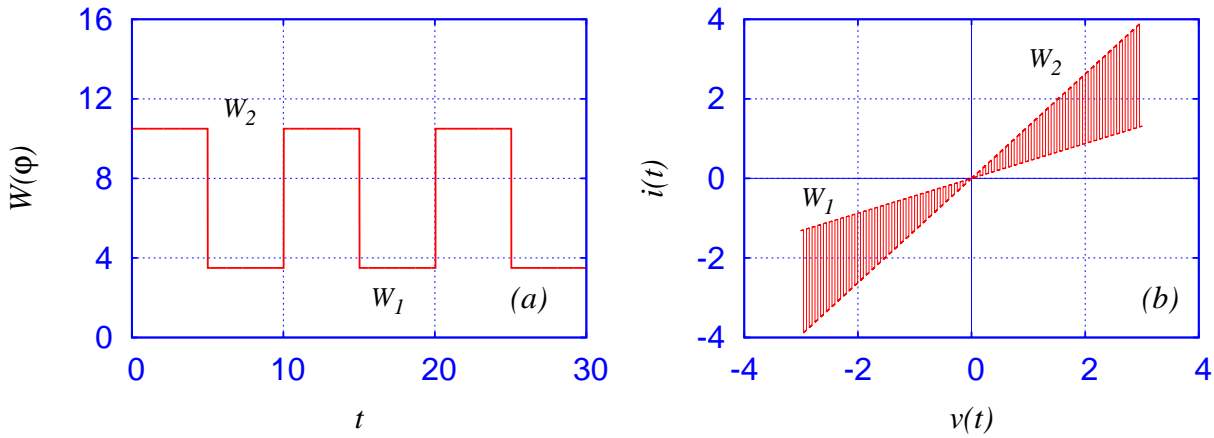


Fig. 1. Memristor Resistive Switching Characteristic:(a) Variation of memductance $W(\phi(t))$ as a function of time t and (b) variations of $(v-i)$ characteristic due to memristor switching.

From Fig. 1(a) we find that the memristor behaves as a practical resistive switching element as postulated by Chua in [Chua, 2011]. The memristor has a very low memductance W_1 during the time $0 < t \leq t_1$ and a very large memductance W_2 during the time $t_1 < t \leq T$. During the time the memductance is low, the memristor switch is said to be open ($S = 0$), while during the time the memductance is high, the switch is said to be closed ($S = 1$). After a period of time T , the switch repeats its operation, that is, the memristor takes on states $S = 0$ and $S = 1$ alternately for $nT < t \leq (n+1)T$, where n is any integer > 1 . As the switching time T of the memristor is inherently very small when compared to mechanical switches, it is suitable for digital applications.

The $(v-i)$ characteristic is obtained by plotting the current $i(t)$ from Eq. (2), as a function of the memristor voltage $v(t)$. This characteristic is a set of two straight lines with slopes equal to the memductance value W_1 when the memristor is in an OFF state and W_2 when in the ON state respectively. Hence the characteristic in the $(v-i)$ plane alternates between these two straight lines as it constantly switches from the OFF state to ON state and vice-versa as shown in Fig. 1(b).

2.2. Memristor Modulation

The current $i(t)$ across the memristor, as is seen from Eq. (2), varies not only with the voltage $v(t)$ applied across it, but also with the memductance $W(\phi(t))$. Let a dc voltage be applied to the memristor such that

$$v(t) = v_{dc}.\quad (8)$$

Then the current across the memristor should possess a time varying nature due to the resistive switching property. This is actually the case as is shown in Fig. 2(a). Let the voltage $v(t)$ driving the memristor be

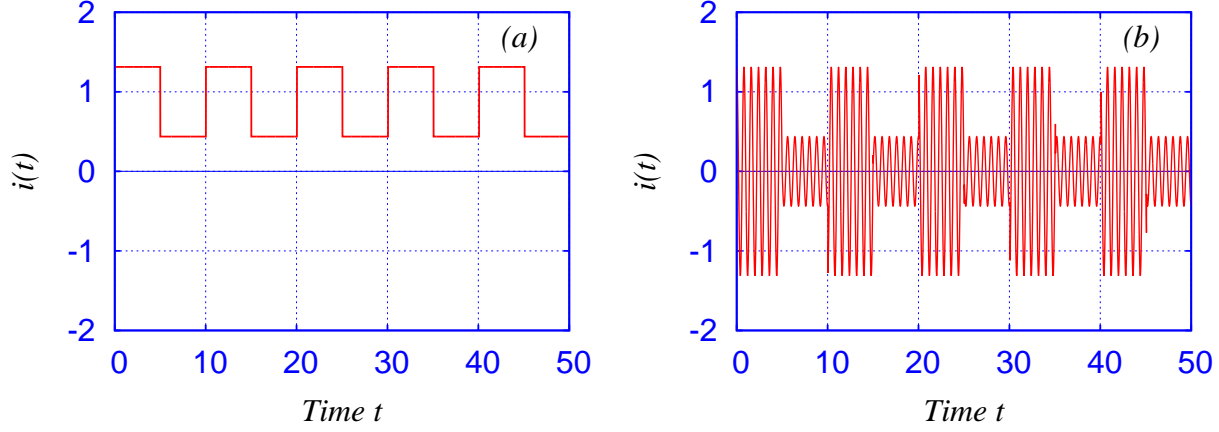


Fig. 2. Memristor Modulation: (a) Variation of the current $i(t)$ across the memristor when a constant potential v_{dc} is applied and (b) the resultant current $i(t)$ when a periodic voltage $v(t) = v_0 \cos(2\pi f_e t)$ is applied. It is clear that the superposed current $i(t)$ in the second case is a modulated current with three frequency components, namely, f_e the frequency of the external force, and two components $f_e \pm (2n - 1)f_m$, $n = 1, 2, 3, \dots$ arising due to the interaction of the external force with the memristor oscillations of frequency f_m .

a periodic voltage, say for example a sinusoid with a frequency f_e , that is

$$v(t) = v_0 \cos(2\pi f_e t). \quad (9)$$

Then on substituting Eqs. (6) and (9) into Eq. (2), the current across the memristor is

$$\begin{aligned} i(t) &= \left\{ W(a) + W(b) \frac{4\Phi_m}{\pi} \sum_{n=1}^{\infty} \frac{\sin((2n-1)2\pi f_m t)}{(2n-1)} \right\} v_0 \cos(2\pi f_e t) \\ &= W(a) v_0 \cos(2\pi f_e t) + \\ &\quad W(b) \frac{4\Phi_m v_0}{\pi} \sum_{n=1}^{\infty} \left\{ \frac{\sin((2n-1)2\pi f_m t)}{(2n-1)} \right\} v_0 \cos(2\pi f_e t) \\ &= W(a) v_0 \cos(2\pi f_e t) + \\ &\quad \left(\frac{4W(b)\Phi_m v_0}{2\pi} \right) \sum_{n=1}^{\infty} \left\{ \frac{\sin(2\pi(f_e + (2n-1)f_m)t)}{(2n-1)} \right\} + \\ &\quad \left(\frac{4W(b)\Phi_m v_0}{2\pi} \right) \sum_{n=1}^{\infty} \left\{ \frac{\sin(2\pi(f_e - (2n-1)f_m)t)}{(2n-1)} \right\}. \end{aligned} \quad (10)$$

Thus we find that in addition to the frequency f_e of the driving voltage, the memristor causes the circuit to generate new currents which are sinusoids with frequencies $(f_e \pm (2n - 1)f_m)$, $n = 1, 2, 3, \dots$. The superposed current of all the sinusoids is shown in Fig. 2(b).

The frequencies of currents across the memristor when it is driven by a constant voltage and a sinusoidal voltage can be found out from power spectral analysis as shown in Fig. 3. The power spectrum of the current across the memristor when it is driven by a constant voltage v_{dc} shows a single peak at f_m and its harmonics. Similarly the power spectrum of the current across the memristor when driven by a sinusoidal voltage shows three prominent peaks, one at the driving frequency f_e , and the other two at $(f_e - f_m)$ and at $(f_e + f_m)$, in addition to the various subharmonic and super harmonic frequency components.

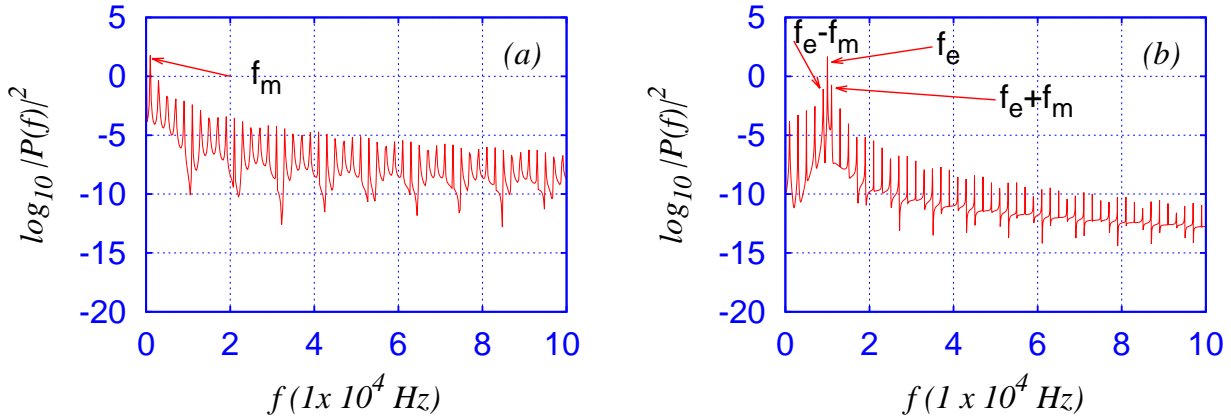


Fig. 3. Power Spectra of Memristor Modulation : Power spectrum of the current $i(t)$ across the memristor (a) showing a single peak at f_m when a constant voltage v_{dc} is applied and (b) showing peaks at f_e and at $f_e \pm (2n-1)f_m$ when a sinusoidal voltage $v(t) = v_0 \cos(2\pi f_e t)$ is applied. The numerical values are: $f_m = 1000\text{Hz}$, $f_e = 10000\text{Hz}$, $(f_e - f_m) = 9000\text{Hz}$ and $(f_e + f_m) = 11000\text{Hz}$.

It is evident from the above discussion that had the memristor possessed a purely time invariant nature, that is, if $W(b) = 0$, it would cause the circuit to generate just a single sinusoid response with the original driving frequency f_e only.

This ability of the memristor to introduce additional frequencies and harmonics in the circuit whenever it is driven by sinusoidal or any other periodic signal causes limit cycle oscillations in memristive circuits to take on a quasiperiodic nature as will be seen in the following sections.

3. Memristive Murali-Lakshmanan-Chua Circuit

A memristive MLC circuit, constructed by replacing the Chua's diode in the classical Murali-Lakshmanan-Chua circuit with an analog model of an active flux controlled memristor, proposed by [Ishaq Ahamed *et al.*, 2011] as its non-linear element was reported earlier in 2013, refer Ishaq & Lakshmanan [2013]. The schematic circuit is shown in Fig. 4, while the actual analog realization based on the prototype model for the memristor is shown in Fig. 5. Applying Kirchoff's laws, the circuit equations can be written as a

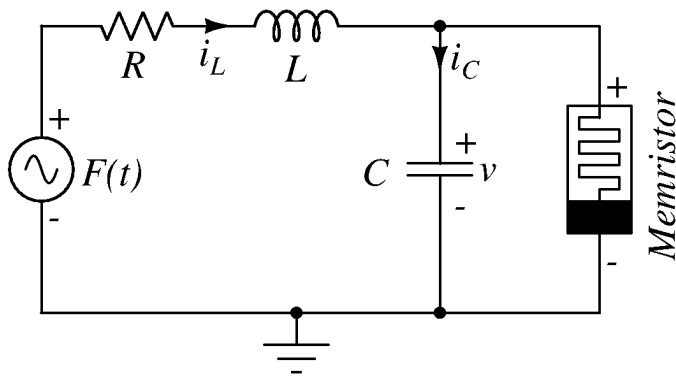


Fig. 4. The memristive MLC circuit

set of autonomous ordinary differential equations (ODEs) for the flux $\phi(t)$, voltage $v(t)$, current $i(t)$ and

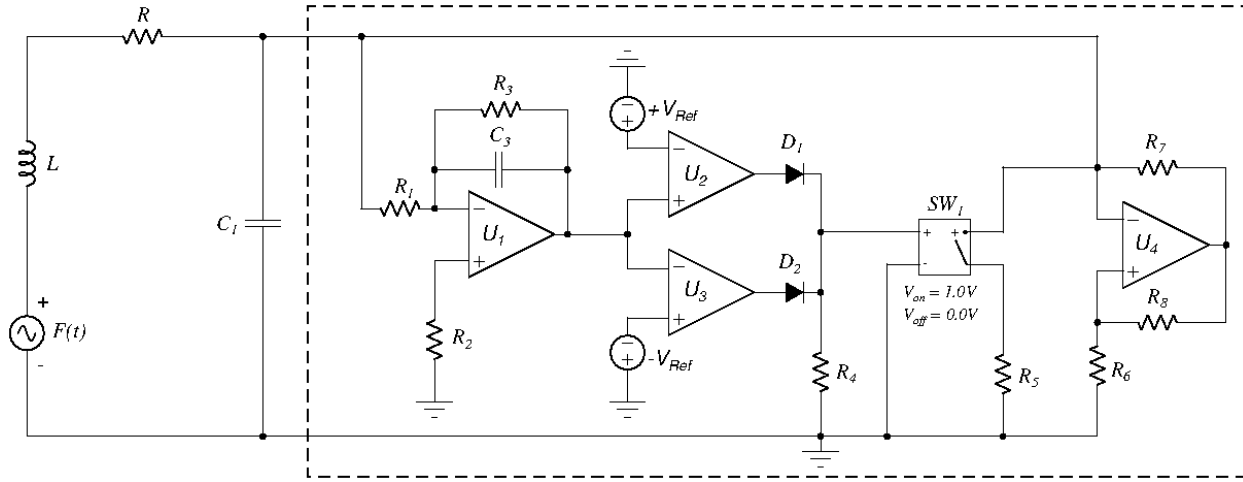


Fig. 5. A Multisim Prototype Model of a memristive MLC circuit. The memristor part is shown by the dashed outline. The parameter values of the circuit are fixed as $L = 21mH$, $R = 900\Omega$, $C_1 = 10.5nF$. The frequency of the external sinusoidal forcing is fixed as $\nu_{ext} = 8.288kHz$ and the amplitude is fixed as $F = 770mV_{pp}$ (peak-to-peak voltage).

the time p in the extended coordinate system as

$$\begin{aligned} \frac{d\phi}{dt} &= v, \\ C \frac{dv}{dt} &= i - W(\phi)v, \\ L \frac{di}{dt} &= -v - Ri + F \sin(\Omega p), \\ \frac{dp}{dt} &= 1. \end{aligned} \quad (11)$$

Here $W(\phi)$ is the memductance of the memristor and is as defined in [Itoh & Chua, 2008],

$$W(\phi) = \frac{dq(\phi)}{d\phi} = \begin{cases} G_{a_1}, & |\phi| > 1 \\ G_{a_2}, & |\phi| \leq 1, \end{cases} \quad (12)$$

where G_{a_1} and G_{a_2} are the slopes of the outer and inner segments of the characteristic curve of the memristor respectively. We can rewrite Eqs. (11) in the normalized form as

$$\begin{aligned} \dot{x}_1 &= x_2, \\ \dot{x}_2 &= x_3 - W(x_1)x_2, \\ \dot{x}_3 &= -\beta(x_2 + x_3) + f \sin(\omega x_4), \\ \dot{x}_4 &= 1. \end{aligned} \quad (13)$$

Here dot stands for differentiation with respect to the normalized time τ (see below) and $W(x_1)$ is the normalized value of the memductance of the memristor, given as

$$W(x_1) = \frac{dq(x_1)}{dx_1} = \begin{cases} a_1, & |x_1| > 1 \\ a_2, & |x_1| \leq 1 \end{cases} \quad (14)$$

where $a_1 = G_{a_1}/G$ and $a_2 = G_{a_2}/G$ are the normalized values of G_{a_1} and G_{a_2} mentioned earlier and are negative. The rescaling parameters used for the normalization are

$$\begin{aligned} x_1 = \frac{G\phi}{C}, x_2 = v, x_3 = \frac{i}{G}, x_4 = \frac{Gp}{C}, G = \frac{1}{R}, \beta = \frac{C}{LG^2}, \\ \omega = \frac{\Omega C}{G} = \frac{2\pi\nu C}{G}, \tau = \frac{Gt}{C}, f = F\beta. \end{aligned} \quad (15)$$

In our earlier work on this memristive MLC circuit, see Ishaq & Lakshmanan [2013], we reported that the addition of the memristor as the nonlinear element converts the system into a piecewise-smooth continuous flow having two discontinuous boundaries, admitting *Grazing bifurcations*, a type of discontinuity induced bifurcation (DIB). These Grazing bifurcations were identified as the cause for the occurrence of hyperchaos, hyperchaotic beats and transient hyperchaos in this memristive MLC system.

As stated in Sec. 1, piecewise-continuous systems possess rich dynamics, and are known to exhibit many types of non-smooth bifurcations, such as *sliding* bifurcations, *stick-slip* oscillations, *impact* oscillations, etc. As the memristive MLC circuit is a piecewise-continuous system, we naturally realized that it can be no exception and that it should exhibit many other hitherto unknown *discontinuity induced* bifurcations. Hence we made further investigations on this system by applying non-smooth bifurcation theory which has been well developed and applied to mechanical systems. These investigations led us to the observation of *sliding* bifurcations and *Discontinuity Induced Hopf* and *Neimark-Sacker* bifurcations thus establishing the robustness and versatility of this simple low dimensional circuit.

4. Memristive MLC Circuit as a Non-smooth System

The memristive MLC circuit is a piecewise-smooth continuous system by virtue of the discontinuous nature of its nonlinearity, namely the memristor. Referring to the memductance characteristic, we find that the memristor switches states at $x_1 = +1$ and at $x_1 = -1$ either from a more conductive ON state to a less conductive OFF state or vice versa. These switching states of the memristor give rise to two discontinuity boundaries or switching manifolds, $\Sigma_{1,2}$ and $\Sigma_{2,3}$ which are symmetric about the origin and are defined by the zero sets of the smooth functions $H_i(\mathbf{x}, \mu) = C^T \mathbf{x}$, where $C^T = [1, 0, 0, 0]$ and $\mathbf{x} = [x_1, x_2, x_3, x_4]$, for $i = 1, 2$. Hence $H_1(\mathbf{x}, \mu) = (x_1 - x_1^*)$, $x_1^* = -1$ and $H_2(\mathbf{x}, \mu) = (x_1 - x_1^*)$, $x_1^* = +1$, respectively. Consequently the phase space \mathcal{D} can be divided into three subspaces S_1 , S_2 and S_3 due to the presence of the two switching manifolds. The memristive MLC circuit can now be rewritten as a set of smooth ODEs

$$\dot{x}(t) = \begin{cases} F_2(\mathbf{x}, \mu), & H_1(\mathbf{x}, \mu) > 0 \text{ \& } H_2(\mathbf{x}, \mu) < 0, \mathbf{x} \in S_2, \\ F_{1,3}(\mathbf{x}, \mu), & H_1(\mathbf{x}, \mu) < 0 \text{ \& } H_2(\mathbf{x}, \mu) > 0, \mathbf{x} \in S_{1,3}, \end{cases} \quad (16)$$

where μ denotes the parameter dependence of the vector fields and the scalar functions. The vector fields F_i 's are

$$F_i(\mathbf{x}, \mu) = \begin{pmatrix} x_2 \\ -a_i x_2 + x_3 \\ -\beta x_2 - \beta x_3 + f \sin(\omega x_4) \\ 1 \end{pmatrix}, i = 1, 2, 3 \quad (17)$$

where we have $a_1 = a_3$.

The discontinuity boundaries $\Sigma_{1,2}$ and $\Sigma_{2,3}$ are not uniformly discontinuous. This means that the degree of smoothness of the system in some domain \mathcal{D} of the boundary is not the same for all points $x \in \Sigma_{ij} \cap \mathcal{D}$. This causes the memristive MLC circuit to behave as a non-smooth system having a degree of smoothness of either *one* or *two*. In such a case it will behave either as a *Filippov system* or as a *piecewise-smooth continuous flow* respectively, refer Appendix A. Hence the memristive MLC circuit is found to admit different types of *Discontinuity Induced Bifurcations* (DIB's) such as *Boundary Equilibrium Bifurcations* (BEB's), *Crossing-Sliding* bifurcations, *Grazing-Sliding* bifurcations, *Switching-Sliding* bifurcations and pure *Grazing* bifurcations. In this paper we restrict our description to the boundary equilibrium bifurcations alone that are admitted by this system. *Boundary Equilibrium Bifurcations* are the simplest type of DIB's that occur in piecewise-smooth continuous systems [di Bernardo *et al.*, 2002; Leine & Campen, 2002; Leine & Nijmeijer, 2004]. They occur if for a particular critical value of the parameter the equilibrium point lies precisely on the discontinuity boundary Σ . In this paper we will show that the replacement of the Chua's diode by an active flux controlled memristor in the MLC circuit results in the system possessing boundary equilibrium points and exhibiting discontinuity induced Hopf and Neimark-Sacker bifurcations about these points. We will analyse the equilibrium points of the circuit, their stability and the dynamics arising from these DIBs in the following sections. We also note here that any other nonsmooth system

having a degree of smoothness two or greater than two can be shown to exhibit similar kind of boundary equilibrium points and associated bifurcations.

4.1. Equilibrium Points and their Stability

In the absence of the driving force, that is if $f = 0$, the memristive MLC circuit can be considered as a three-dimensional autonomous system with vector fields given by

$$F_i(\mathbf{x}, \mu) = \begin{pmatrix} x_2 \\ -a_i x_2 + x_3 \\ -\beta x_2 - \beta x_3 \end{pmatrix}, i = 1, 2, 3. \quad (18)$$

This three dimensional autonomous system has a trivial equilibrium point E_0 , two *admissible equilibrium* points E_{\pm} and two *boundary equilibrium* points $E_{B\pm}$ (see Appendix A for details). The multiplicity of equilibrium points arises because of the non-smooth nature of the nonlinear function, namely $W(x_1)$ given in Eq. (14). The trivial equilibrium point is given as

$$E_0 = \{(x_1, x_2, x_3) | x_1 = x_2 = x_3 = 0\} \quad (19)$$

The two admissible equilibria E_{\pm} are

$$E_{\pm} = \{(x_1, x_2, x_3) | x_2 = x_3 = 0, x_1^* = \text{constant and not equal to } \pm 1\} \quad (20)$$

At the admissible equilibrium points E_{\pm} , the conditions given by Eqs. (A.4) and (A.5) are satisfied, that is

$$\begin{aligned} F_1(\mathbf{x}, \mu) &= 0, \\ H_1(\mathbf{x}, \mu) &:= \lambda_1 < 0, \end{aligned} \quad (21)$$

or

$$\begin{aligned} F_3(\mathbf{x}, \mu) &= 0, \\ H_2(\mathbf{x}, \mu) &:= \lambda_2 > 0. \end{aligned} \quad (22)$$

As the vector fields $F_1(\mathbf{x}, \mu)$ and $F_3(\mathbf{x}, \mu)$ are symmetric about the origin, that is $F_1(\mathbf{x}, \mu) = F_3(-\mathbf{x}, \mu)$, the admissible equilibria E_{\pm} are also placed symmetric about the origin in the subspaces S_1 and S_3 . These are shown in Fig. 6 for a certain choice of parametric values. For plotting the stable focus E_+ in S_3 we assumed the initial conditions as $x_1 = 0.0$, $x_2 = 0.01$, $x_3 = 0.01$ while for the stable focus E_- in the subspace S_1 the initial conditions are $x_1 = 0.0$, $x_2 = -0.01$, $x_3 = -0.01$.

At the boundary equilibrium points $E_{B\pm}$,

$$E_{B\pm} = \{(x_1, x_2, x_3) | x_2 = x_3 = 0, \hat{x}_1 = \pm 1\} \quad (23)$$

the conditions given by Eq. (A.5) are satisfied, namely

$$\begin{aligned} F_{1,2}(\hat{\mathbf{x}}, \mu) &= 0, & H_1(\hat{\mathbf{x}}, \mu) &= 0 & \text{or} \\ F_{2,3}(\hat{\mathbf{x}}, \mu) &= 0, & H_2(\hat{\mathbf{x}}, \mu) &= 0 \end{aligned} \quad (24)$$

These boundary equilibria lie on the switching manifolds $\Sigma_{1,2}$ and $\Sigma_{2,3}$.

The definitive conditions for the existence of equilibria given above however do not tell us about the stability of these equilibrium states. Therefore we construct the Jacobian matrices N_i , $i = 1, 2, 3$ and evaluate their eigenvalues at these points to analyse their stability,

$$N_i = \begin{pmatrix} 0 & 1 & 0 \\ 0 & -a_i & 1 \\ 0 & -\beta & -\beta \end{pmatrix}, i = 1, 2, 3. \quad (25)$$

The characteristic equation associated with the system N_i in these equilibrium states is

$$\lambda^3 + p_2 \lambda^2 + p_1 \lambda = 0, \quad (26)$$

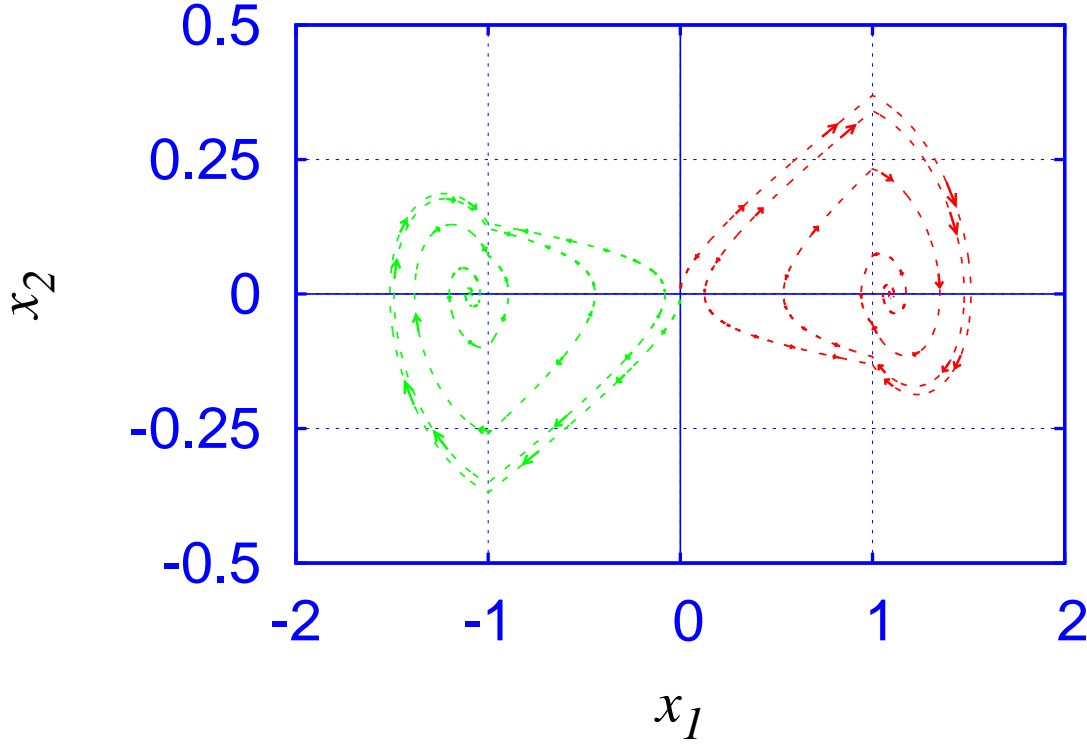


Fig. 6. Figure showing the equilibrium points E_{\pm} in the subspaces S_1 and S_3 for the parameter value above $\beta_c = 0.8250$. The initial conditions are $x_1 = 0.0$, $x_2 = 0.01$, $x_3 = 0.01$ for the fixed point E_+ in the subspace S_3 and $x_1 = 0.0$, $x_2 = -0.01$, $x_3 = -0.01$ for the fixed point E_- in the subspace S_1 .

where λ 's are the eigenvalues that characterize the equilibrium states and p_i 's are the coefficients, given as $p_1 = \beta(1 + a_i)$ and $p_2 = (\beta + a_i)$. The eigenvalues are

$$\lambda_1 = 0, \lambda_{2,3} = \frac{-(\beta + a_i)}{2} \pm \frac{\sqrt{(\beta - a_i)^2 - 4\beta}}{2}. \quad (27)$$

where $i = 1, 2, 3$. Depending on the eigenvalues, the nature of the equilibrium states differ.

- (1) When $(\beta - a_i)^2 = 4\beta$, the equilibrium state will be a stable/unstable star depending on whether $(\beta + a_i)$ is positive or not.
- (2) When $(\beta - a_i)^2 > 4\beta$, the equilibrium state will be a saddle.
- (3) When $(\beta - a_i)^2 < 4\beta$, the equilibrium state will be a stable/unstable focus.

For the third case, the circuit admits self oscillations with natural frequency varying in the range $\sqrt{[(\beta - a_1)^2 - 4\beta]}/2 < \omega_o < \sqrt{[(\beta - a_2)^2 - 4\beta]}/2$. It is at this range of frequency that the memristor switching also occurs.

4.2. Boundary Equilibrium Bifurcations (BEB)

The boundary equilibrium bifurcations are analogous to the border-collision bifurcations in maps. For a piecewise smooth continuous flow, two types of boundary equilibrium bifurcations have been observed, namely *persistence* and *non-smooth fold*, see [di Bernardo *et al.*, 2008] and the references mentioned therein. The conditions for the existence of these bifurcations are given in Appendix - A. Applying them, we find that

the memristive MLC circuit does not admit any *boundary equilibrium* bifurcations. This can be explained as due to the non-invertibility of the Jacobian matrices.

Let us linearise the memristive MLC circuit described by the Eqs. (16) and (17) about the boundary equilibrium points $E_{B\pm}$ as referred to in Eqs (A.9) and (A.10) in Appendix A, that is

$$\begin{aligned} N_1 \mathbf{x}^- + M_1 \mu &= 0, \\ C^T \mathbf{x}^- + D \mu &= \lambda^-, \end{aligned} \quad (28)$$

and

$$\begin{aligned} N_2 \mathbf{x}^+ + M_2 \mu &= N_1 \mathbf{x}^+ M_1 \mu + E \lambda^+ = 0, \\ C^T \mathbf{x}^+ + D \mu &= \lambda^+, \end{aligned} \quad (29)$$

where $N_1 = F_{1,x}$, $M_1 = F_{1,\mu}$, $C^T = H_x$, $D = H_\mu$ and $\mathbf{x}^+(\mu)$ and $\mathbf{x}^-(\mu)$ are the branches of the equilibria, before and after the crossing of the discontinuity boundaries at $\mu = \mu^*$ in the subspaces S_1 and S_2 of the vector fields $F_1(\mathbf{x}, \mu)$ and $F_2(\mathbf{x}, \mu)$ respectively. Then

$$\begin{aligned} \begin{pmatrix} 0 & 1 & 0 \\ 0 & -a_1 & 1 \\ 0 & -\beta & -\beta \end{pmatrix} \mathbf{x}^- + \begin{pmatrix} 0 \\ 1 \\ 1 \end{pmatrix} \mu &= 0 \\ \begin{pmatrix} 1 \\ 0 \\ 0 \end{pmatrix} \mathbf{x}^- + D \mu &= \lambda^-, \end{aligned} \quad (30)$$

and

$$\begin{aligned} \begin{pmatrix} 0 & 1 & 0 \\ 0 & -a_1 & 1 \\ 0 & -\beta & -\beta \end{pmatrix} \mathbf{x}^+ + \begin{pmatrix} 0 \\ 1 \\ 1 \end{pmatrix} \mu + \begin{pmatrix} 0 \\ a_1 - a_2 \\ 0 \end{pmatrix} \lambda^+ &= 0, \\ \begin{pmatrix} 1 \\ 0 \\ 0 \end{pmatrix} \mathbf{x}^+ + D \mu &= \lambda^+. \end{aligned} \quad (31)$$

where we have taken $N_2 - N_1 = E$, with $E = \begin{pmatrix} 0 \\ a_1 - a_2 \\ 0 \end{pmatrix}$. Thus we find that as Eqs. (30) and (31) are satisfied, the system possess two admissible equilibrium points E_{\pm} .

However as the determinant of the Jacobian matrix N_1 is zero, that is as $\det(N_1) = 0$, we find that the Jacobian matrix is not invertible. Consequently the conditions, refer Eqs. (A.9), (A.10), (A.12) and (A.14) for the occurrence of *boundary equilibrium* bifurcations are not satisfied. Therefore based on this we conclude that *boundary equilibrium* bifurcations are not admitted by the memristive MLC circuit.

The non-invertibility of the Jacobian matrices, however suggests that one or more of the many equilibrium points may be *non-hyperbolic* and may admit local bifurcations with respect to one of the vector fields, either F_1 , F_2 or F_3 . This is exactly what happens in the memristive MLC circuit, for we find that *discontinuity induced Hopf* bifurcations and *discontinuity induced Neimark-Sacker* bifurcations occur leading to complex dynamics. As noted earlier, this system can also exhibit even more complicated bifurcations like sliding bifurcations, apart from the grazing bifurcations reported in our earlier work, [Ishaq & Lakshmanan, 2013]. These more sophisticated bifurcations will be reported separately.

5. Discontinuity Induced Hopf Bifurcation

The existence of invariant sets, other than equilibrium points, and their creation and destruction in a boundary equilibrium bifurcation has been reported in [Leine *et al.*, 2000],[Leine & Nijmeijer, 2004] and [Leine & Campen, 2002]. Here in the memristive MLC circuit, as boundary equilibrium bifurcations are not observed, we find that perturbing the boundary equilibrium point about either of the switching manifolds $\Sigma_{1,2}$ or $\Sigma_{2,3}$ results in the trajectory forming a *quasi-periodic* attractor. The birth of the quasi-periodic attractor can be attributed to the occurrence of a *discontinuity induced Hopf* bifurcation at the switching manifolds and *memristor modulation*. Such discontinuity induced Hopf bifurcations leading to *limit cycle* motion in planar non-smooth systems were reported for the first time by Leine & Campen [2006] and in the Chua's oscillator in two separate works by Zhang & Bi [2012] and Fu *et al.* [2015]. For identifying this we apply the extension of the concept of Clarke's generalised differential to Jacobian matrices in order to evaluate mathematically the correct eigenvalues, and have also constructed proper discontinuity mappings such as the *Zero Time Discontinuity Map* (ZDM) and *Poincaré Discontinuity Map* (PDM). The details of these discontinuity mapping corrections have been elaborated in our earlier work, see [Ishaq & Lakshmanan, 2013], and are therefore not provided here for the sake of brevity.

Let us assume the normalised parameter values of the memristor MLC circuit to be $a_{1,3} = -0.55$, $a_2 = -1.02$. Let β be the control parameter. For the value $\beta = 0.825$, the eigenvalues of the Jacobian matrix N_2 for the subspace S_2 in the central region are $\lambda_{2,1} = 0$, $\lambda_{2,2} = 0.258765$ and $\lambda_{2,3} = -0.0637645$, while the eigenvalues of the Jacobian matrices $N_{1,3}$ for the subspaces in the outer two regions, namely S_1 and S_3 are $\lambda_{(1,3)1} = 0$, $\lambda_{(1,3)2,3} = -0.1375 \pm i 0.5935861$. Looking at the eigenvalues of the Jacobian matrices we find that the trivial equilibrium point E_0 in the subspace S_2 is an unstable *saddle* while the admissible points E_{\pm} in the subspaces S_1 and S_3 are *stable foci* for these parametric values, refer Fig. 6.

Left to themselves, the stability of these equilibrium points will remain unaffected. But when the trajectories cross the switching manifolds $\Sigma_{1,2}$ and $\Sigma_{2,3}$ their behaviour is affected by the vector fields F_1 and F_2 on both sides of the switching boundaries. The combined effect of the two vector fields is so as to cause the birth of periodic orbits.

The evolution of non-smooth dynamics near the switching discontinuities may be investigated by setting up a generalised Jacobian matrix N_q at the equilibrium point E_0 , refer Leine & Campen [2006]. This generalized Jacobian matrix is a set-valued matrix and is given as $N_q = qN_2 + (1 - q)N_{1,3}$, $q \in [0, 1]$. When written explicitly we have

$$N_q = \begin{pmatrix} 0 & 1 & 0 \\ 0 & ((a_1 - a_2)q - a_1) & 1 \\ 0 & -\beta & -\beta \end{pmatrix}. \quad (32)$$

When the auxiliary variable $q = 0$, then from Eq. (32), we find that $N_q = N_{1,3}$. The eigenvalues λ_q in this case therefore reduce to the eigenvalues of the Jacobian matrices $N_{1,3}$ in the outer regions, namely $\lambda_{(1,3)1} = 0.0$ and $\lambda_{(1,3)2,3} = -0.1375 \pm j 0.5935861$. On the other hand, if $q = 1.0$, then from Eq. (32), we find that $N_q = N_2$. Hence the eigenvalues λ_q reduce to the eigenvalues of the Jacobian matrix N_2 in the central region, namely $\lambda_{(2)1} = 0.0$ and $\lambda_{(2)2} = 0.258765$ and $\lambda_{(2)3} = -0.0637645$. These are shown enclosed by circles in Fig. 7.

For other intermediate values of the auxiliary variable q , the eigenvalues λ_q of the generalised Jacobian are set-valued $\lambda_q, q \in [0, 1]$ and form a one-dimensional path in the complex plane. Following this one dimensional path, we find that the eigenvalues become purely imaginary, namely $\lambda_{qi} \simeq \pm j 0.37997$, where $i = 1, 2$ and $j = \sqrt{-1}$ is the imaginary unit. These generalised eigenvalues λ_{qi} are shown by arrows in Fig. 7 and are found to jump through the imaginary axis as a conjugate pair at $q = 0.41480$, thereby suggesting the occurrence of a discontinuous Hopf bifurcation. This bifurcation, though discontinuous, behaves very much like a continuous Hopf bifurcation found in smooth dynamical systems.

For the parameters of the memristive MLC circuit mentioned above, the one parameter bifurcation diagram in the $(\beta - x_2)$ plane and the Lyapunov spectrum are plotted as a function of β , for the range $0.6 < \beta < 1.2$. These are shown in Figs. 8 (a) and 8 (b) respectively. The bifurcation diagram was obtained by constructing the *two-sided Poincaré Map* P_{\pm} , refer Parker & Chua [1984]. As the parameter β is reduced from $\beta = 1.2$, the bifurcation diagram shows a fixed point behaviour for the system. At a critical value

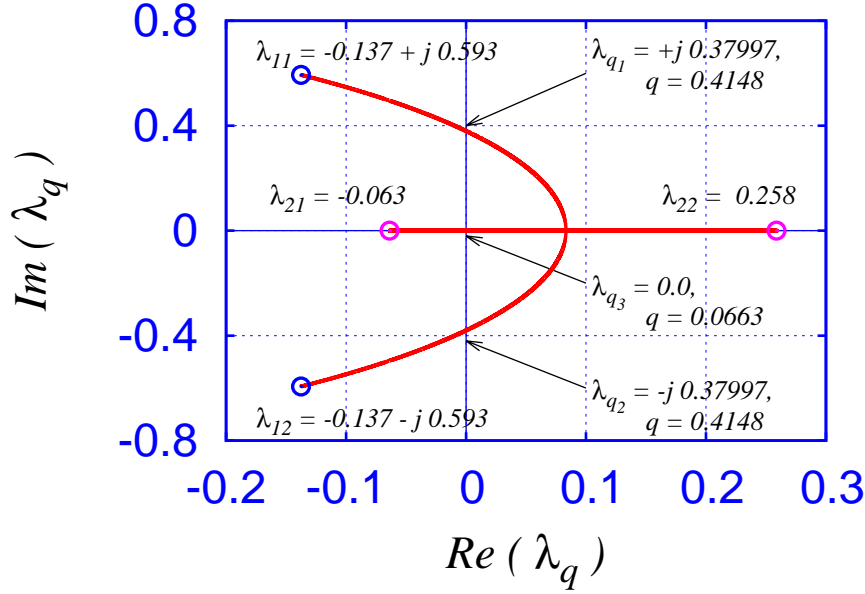


Fig. 7. The one-dimensional path of the generalised eigenvalues λ_q 's in the complex plane parametrised by the auxiliary variable q , showing the jump of the eigenvalues (indicated by arrows) as a conjugated pair at $q = 0.4148$, signalling a *discontinuous Hopf* bifurcation. Also a third crossing of the eigenvalue with the imaginary axis occurring for $q = 0.0663$, indicating a *multiple crossing* bifurcation. For the extreme values of the auxiliary variable, namely $q = 0$ and $q = 1$, the generalised eigenvalues get reduced to the eigenvalues of either of the Jacobian matrices $N_{1,3}$ or N_2 in the outer and inner subspaces of the phase space, respectively, and are shown encircled.

$\beta_c = 0.8250$, the fixed points lose their stability and a bifurcation is observed suggesting the creation of periodic motion. This behaviour continues till $\beta = 0.6$. The Lyapunov spectrum shows that for the control parameter less than the critical value $\beta_c = 0.8250$, the Lyapunov exponents are $\lambda_1 \simeq \lambda_2 = 0.0$ and $\lambda_3 < 0.0$, thereby suggesting that what is observed is in fact quasi-periodic motion.

Referring back to the phase portraits shown in Fig. 6, for $\beta_c = 0.8250$, we find that the system has equilibrium points E_{\pm} , which are *stable foci* in the subspaces S_1 and S_3 as suggested by the eigenvalues for the Jacobian matrices $N_{1,3}$. As the eigenvalues for the Jacobian matrix N_2 suggest an unstable equilibrium, namely a *saddle*, the equilibrium point E_0 in the subspace S_2 repels the trajectories away from it, causing them to cross the switching boundaries $\Sigma_{1,2}$ and $\Sigma_{2,3}$ and settle down to either E_+ in S_3 or to E_- in S_1 respectively. This is the picture observed for control parameter β values less than the critical value $\beta_c = 0.8250$. For the control parameter values less than this critical value, $\beta_c = 0.8250$, we observe quasi-periodic behaviour as shown in Fig. 9(a). These quasi-periodic trajectories pass through all the three subspaces of the state space and enclose the equilibrium points E_{\pm} , shown in Fig. 6, as well. The corresponding power spectrum of the x_2 variable, shown in Fig. 9(b), contains Dirac delta peaks which clearly points to quasi-periodic behaviour.

5.1. Explanation of Quasi-periodic Behaviour

Though the eigenvalues for the generalised Jacobian matrix N_q point to a limit cycle motion alone, the quasi-periodicity exhibited by the system can be explained on the basis of the circuit theoretic properties of the memristor demonstrated in Sec. 2. The discontinuous Hopf bifurcation leads to the birth of periodic motion resulting in self oscillations in the circuit. However the *linear-time varying* property of the memristor gives rise to memristor switching. The interaction of the self oscillations and the memristor switching leads to *memristor induced modulation* which introduces additional frequencies and their harmonics, thereby causing quasi-periodic motion.

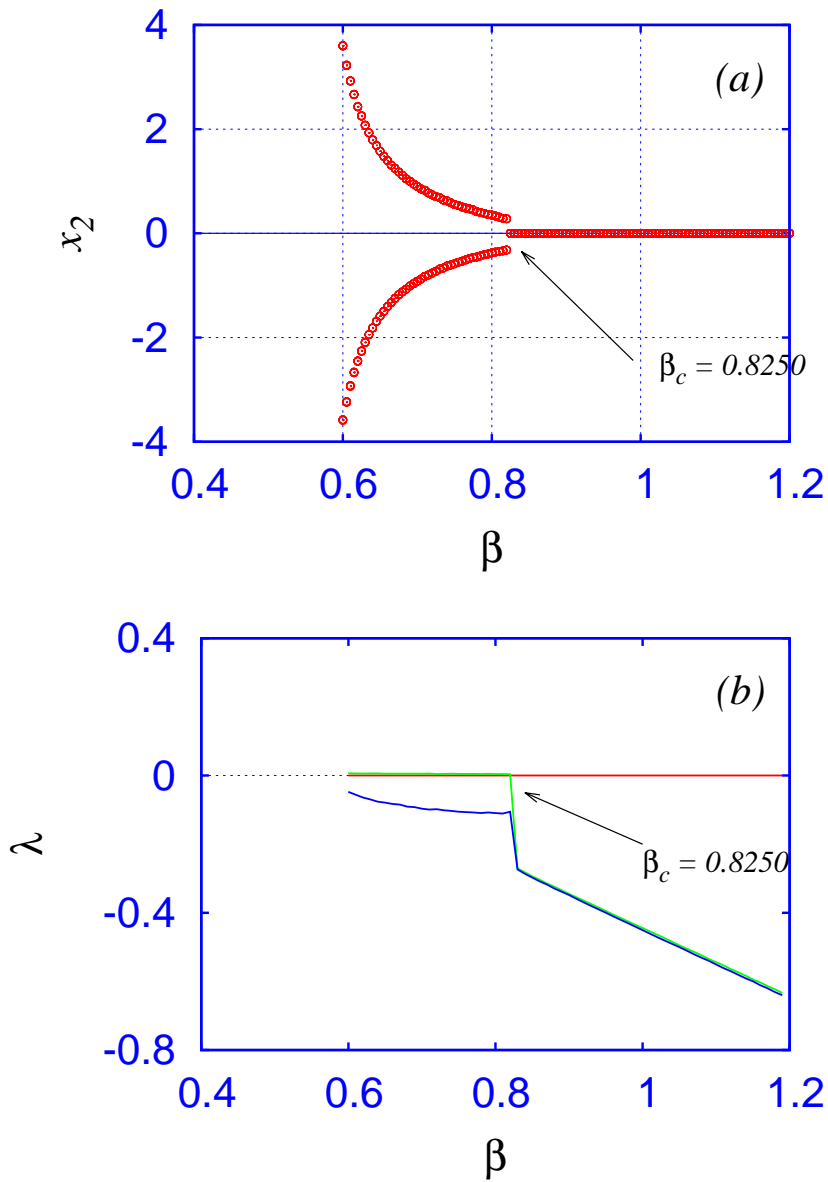


Fig. 8. (a) The one parameter bifurcation diagram in the $(\beta - x_2)$ plane showing the occurrence of discontinuous Hopf bifurcation causing the fixed points E_{\pm} to lose their stability at the critical value $\beta_c = 0.8250$ and resulting in the birth of periodic orbits. (b) The Lyapunov spectrum in the $(\lambda - \beta)$ plane corroborating the above inference. The normalised parameters for the circuit are chosen as $a_{1,3} = -0.55$ and $a_2 = -1.02$.

Referring to Fig. 7 once again, we find that in addition to the the eigenvalues jumping the imaginary axis as a conjugate pair, we find that a third generalised eigenvalue of the system λ_{q3} crosses the imaginary axis at the origin for $q = 0.0663$. Hence we find a *pitch-fork* like bifurcation scenario. This resulting discontinuity induced bifurcation is called *multiple crossing* bifurcation [Leine & Campen, 2006] in the literature, because the eigenvalues cross the imaginary axis more than once during their jump.

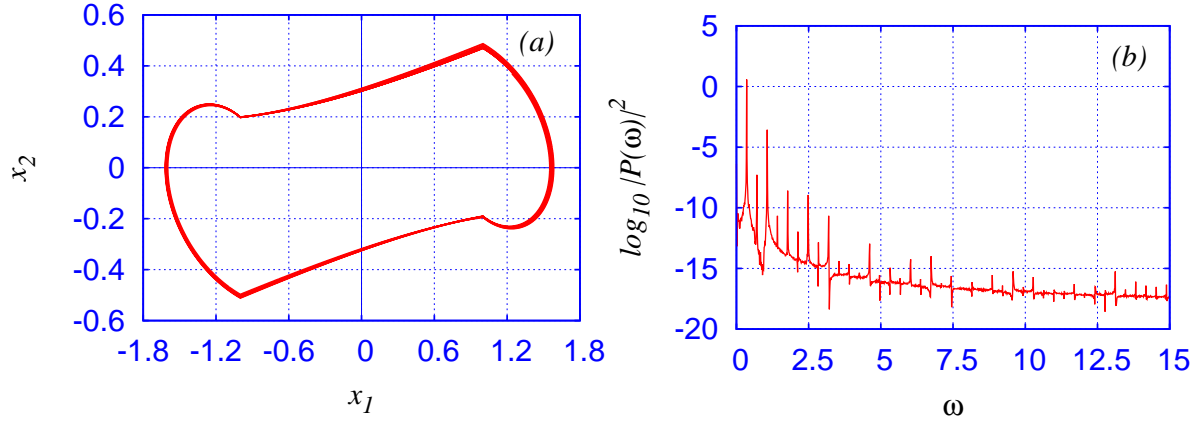


Fig. 9. (a) The phase portrait showing the quasi-periodic orbits arising due to discontinuous Hopf bifurcation, for parameter values below the critical limit $\beta_c = 0.825$. (b) The corresponding power spectrum of the x_2 variable contains Dirac delta peaks, confirming the quasi-periodic behaviour.

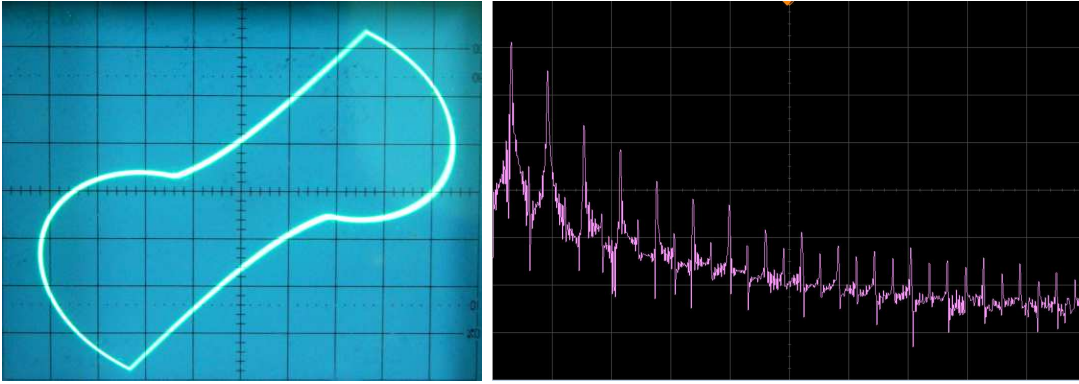


Fig. 10. Figure showing (a) the experimental phase portrait of the quasi-periodic motion arising due to discontinuous Hopf bifurcation, corresponds well to the to the numerical phase portrait in Fig. 6. The experimental values of the circuit elements are $L = 300$ mH, $C = 40$ nF and $F = 0$, that is no external periodic forcing is applied and (b) the power spectrum of the voltage across the capacitor v_c , corresponding to the numerical spectrum shown in Fig. 9, contain Dirac delta peaks, confirming the occurrence of quasi-periodic motion.

5.2. Experimental Observations

The analog circuit of the memristive MLC oscillator shown in Fig. 5 has been implemented in the laboratory using off the shelf components. Here the integrator, the window comparator as well as the negative impedance converter for the memristive part have been implemented using TL081 operational amplifiers. The electronic switch *AD7510DJ* has been used for realizing the switching action. The reason for using TL081 is that it operates at high frequency ranges, has high slew rate and does not show hysteretic behaviour. For the integrator part, the parameters are chosen as $R_1 = 10K\Omega$, $R_2 = 100K\Omega$, $R_3 = 100K\Omega$ and $C_3 = 2.2nF$. For the window comparator part the output resistance is selected as $R_4 = 10K\Omega$, while the reference voltages for are fixed as $\pm 1V$. Further we have selected the linear resistances $R_5 = 1450\Omega$ and $R_6 = 1050\Omega$, $R_7 = 2K\Omega$ and $R_8 = 2K\Omega$ for the negative conductance. The experimental observations were made by employing a Hewlett-Packard Arbitrary Function Generator (33120A) of frequency 15 MHz, an Agilent Mixed Storage Oscilloscope (MSO6014A) of frequency 100 MHz and sampling rate of 2 Giga Samples / seconds. The experimentally obtained phase portrait for quasi-periodic oscillations arising due to Hopf Bifurcation and the experimental power spectrum corresponding to the voltage across the capacitor, v_c are shown in Fig. 10. The parametric values chosen are $L = 300mH$, $C = 40nF$ and when the external

force is switched OFF, that is $F = 0$. Obviously we find that the quasi-periodic behaviour results due to discontinuity induced Hopf bifurcations. We find that the experimental phase portrait and the power spectrum agree well with the numerical behaviour shown in Figs. 9.

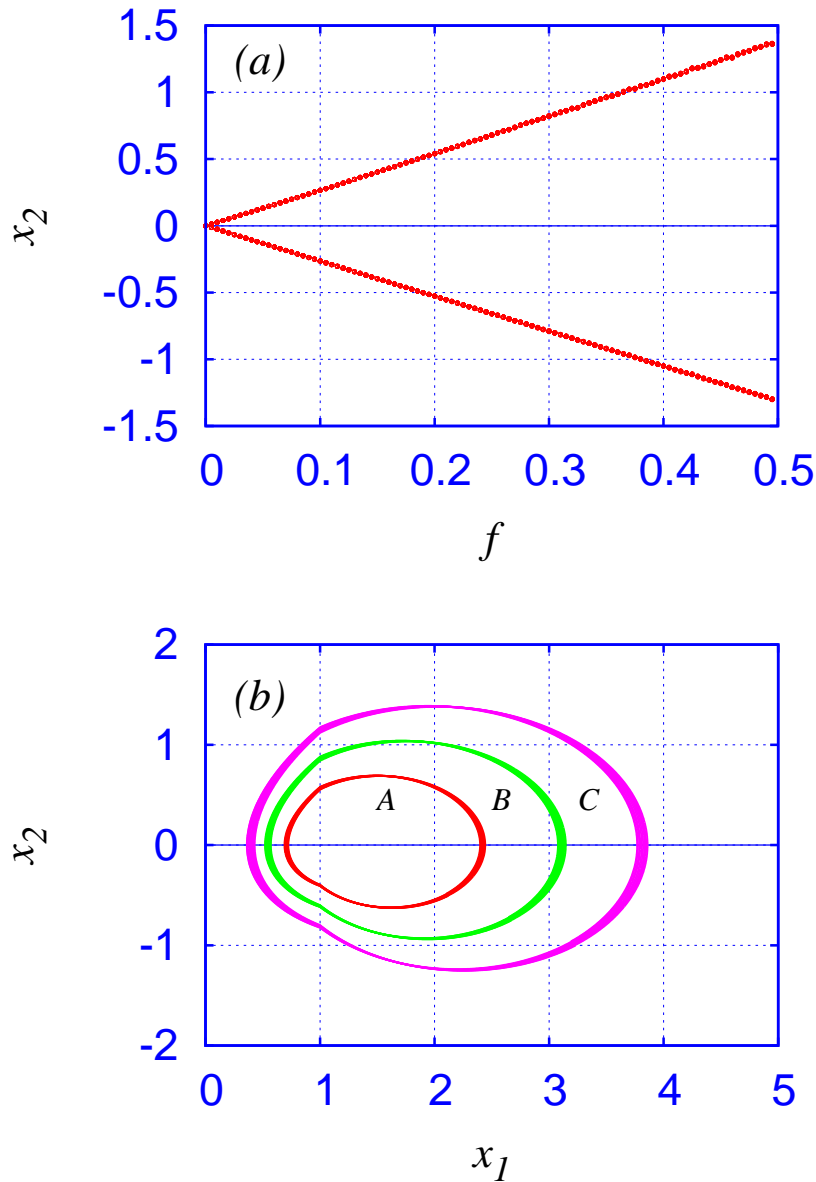


Fig. 11. (a) Bifurcation in the $(f - x_2)$ plane and (b) Phase portraits in the $(x_1 - x_2)$ plane showing the amplitude scaling of the orbits due to forced oscillations with the amplitude of the external force. For the forcing amplitudes $f = 0.2$ 0.3 and 0.4, the forced periodic orbits are named as A, B and C respectively. We find that the area of these orbits scale as $A < B < C$ in accordance with the forcing amplitudes.

6. Amplitude Scaling of Forced Oscillations

In the previous sections we have considered the unforced case of the memristive MLC circuit, that is the case when $f = 0$. Here, in this section, we show that when an external sinusoidal forcing is included, the circuit admits forced oscillations that may be quasi-periodic, chaotic or hyperchaotic depending on the vector fields F_i 's.

We have seen that the admissible equilibrium points E_{\pm} for the memristive MLC circuit are asymptotically stable for control parameter values above the Hopf bifurcation value β_c in the absence of external force. However when external periodic excitation of amplitude f is applied, we find that though the circuit does not undergo any boundary equilibrium bifurcations (BEBs), these admissible equilibrium points E_{\pm} become unstable and give birth to periodic/quasiperiodic oscillations. The amplitudes of these orbits are found to scale linearly with the amplitude of the external force f .

The parameters of the circuit are chosen to be the same as in the autonomous case, that is $a_1 = -0.55$, $a_2 = -1.02$, $\beta = 1.0$ with the frequency of the periodic oscillations as $\omega = 0.75$. A bifurcation diagram is drawn by taking the intersections of the periodic orbits with a *two-sided Poincarè section* P_{\pm} . Figure 11(a) shows the bifurcation diagram in the $(f - x_2)$ plane wherein the amplitude of the quasi-periodic orbits scale with the amplitude f of the external force for the range $0 < f < 0.5$. This is shown more explicitly in the phase diagrams in Fig. 11(b). Here the phase portraits in the $(x_1 - x_2)$ plane for the forcing amplitudes $f = 0.2, 0.3$ and 0.4 are plotted and are named as A, B and C respectively. We find that the area of the orbits scale as $A < B < C$ in accordance with the forcing amplitudes.

7. Discontinuity Induced Neimark-Sacker Bifurcations

The memristive MLC circuit which is found to exhibit forced oscillations with a frequency equal to the external forcing frequency ω_{ext} , undergoes what is called as the *discontinuity induced secondary Hopf* bifurcations or *discontinuity induced Neimark-Sacker* bifurcations as the control parameter β is varied. Generally Neimark-Sacker bifurcations are found to give rise to *two-frequency* quasi-periodic solutions. However in this circuit, due to the presence of memristor modulation, *n-frequency* quasi-periodic solutions are generated. According to Floquet theory, the occurrence of this type of bifurcations can be explained by setting up the *variational equation* for the system and determining the *characteristic multipliers* of the *monodromy matrix*.

The variational equation is a matrix-valued time-varying linear differential equation. It is the linearisation of the vector field along the trajectory of the system. For smooth dynamical systems defined by

$$\dot{\mathbf{x}} = F(\mathbf{x}, t), \quad \mathbf{x}(t_0) = \mathbf{x}_0 \quad (33)$$

the variational equation is given as, refer Parker & Chua [1984],

$$\begin{aligned} \dot{\Phi}_t(\mathbf{x}_0, t_0) &= D_x F(\phi_t(\mathbf{x}_0, t_0), t) \Phi_t(\mathbf{x}_0, t_0), \\ \Phi_{t_0}(\mathbf{x}_0, t_0) &= I. \end{aligned} \quad (34)$$

where $\phi_t(\mathbf{x}_0, t_0)$ is the *flow function*. Here $\phi_t(\mathbf{x}_0, t_0)$ is the solution of the Eq. (33), that is $\phi_t(\mathbf{x}_0, t_0) = x_0$. Further

$$\begin{aligned} \Phi_t(\mathbf{x}_0, t_0) &:= D_{x_0} \phi_t(\mathbf{x}_0, t_0), \\ \Phi_{t_0}(\mathbf{x}_0, t_0) &:= D_{x_0} \phi_{t_0}(\mathbf{x}_0, t_0). \end{aligned} \quad (35)$$

Here D_x stands for vector differentiation and I is the identity matrix.

The eigenvalues of the monodromy matrix are called *characteristic multipliers* or *Floquet multipliers* and are usually denoted as m_i 's. Just as the eigenvalues λ_i 's of the Jacobian matrix determine the stability of the equilibrium points of the system, the characteristic multipliers m_i 's of the monodromy matrix determine the stability of the periodic solutions.

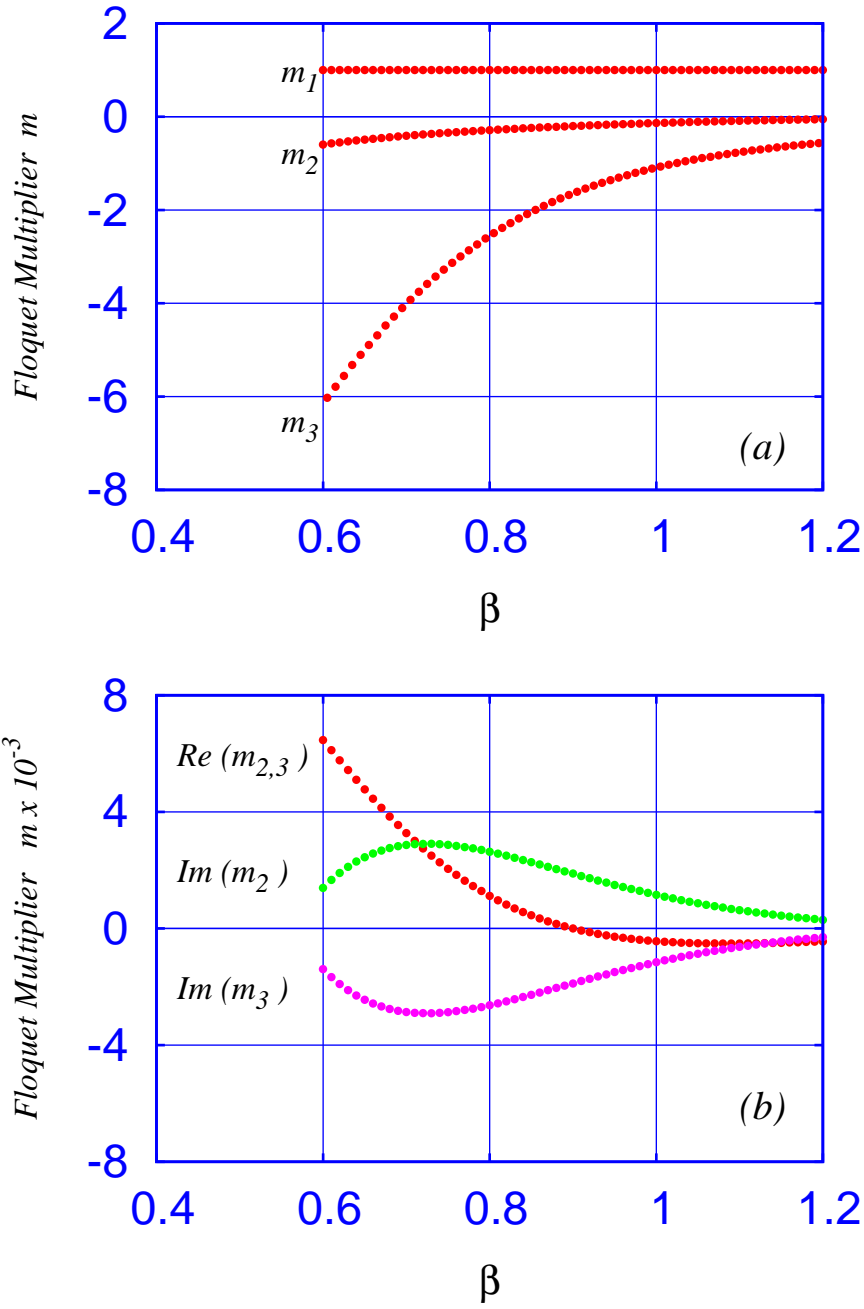


Fig. 12. Variation of (a) the characteristic multipliers m_i 's of the monodromy matrix for the range $0.6 < \beta < 1.2$ and of (b) the generalised characteristic multipliers m_{q_i} 's for the same range. In both the cases one of the multipliers is unity. The crossing of the real part of $m_{q_{2,3}}$ at the critical value $\beta_m = 0.9$ signals discontinuity induced Neimark-Sacker bifurcation.

For a piecewise-smooth system, having a single switching manifold $\Sigma_{1,2}$, defined by the zero vlaue of the scalar function $H(\mathbf{x})$, the state equations are

$$\dot{\mathbf{x}} = \begin{cases} F_1(\mathbf{x}, t) & \text{if } H(\mathbf{x}) < 0, \\ F_2(\mathbf{x}, t) & \text{if } H(\mathbf{x}) > 0. \end{cases} \quad (36)$$

As the vector fields F_i 's for $i = 1, 2$ are discontinuous at the switching boundaries $\Sigma_{1,2}$, the gradient $D_x F(\phi_t(\mathbf{x}_0, t_0), t)$ does not exist when $x(t) \in \Sigma_{1,2}$. The crossing of the switching boundary $\Sigma_{1,2}$ by the solution $x(t)$ at an instance of time, say t_p causes the monodromy matrix to jump at this switching boundary.

Using the concept of generalised differential of Clarke, we saw that the generalisation of a Jacobian matrix $N_{1,2}$ around an equilibrium point of a non-smooth system gave rise to a set-valued generalised Jacobian matrix N_q , $q \in [0, 1]$, whose eigenvalues are also set-valued, that is λ_{qs} , $q \in [0, 1]$. These set-valued eigenvalues λ_{qs} were able to explain correctly the behaviour of the non-smooth system at the switching boundaries.

The monodromy matrix is a linearisation of the periodic solution and therefore for all practical purposes be considered as a Jacobian matrix for periodic orbits. Hence in a manner similar to the construction of a generalised Jacobian, Leine & Campen [2006] had extended the concept of generalisation to the monodromy matrix also, constructing thereby a set-valued monodromy matrix, say Q . This set-valued monodromy matrix is called in the literature of nonsmooth systems as the *Saltation Matrix*. The eigenvalues of the Saltation matrix will also be set-valued and are called the generalised characteristic multipliers m_{q_i} 's. The crossing of the imaginary axis of these characteristic multipliers as a conjugate pair in the eigen space will then cause the periodic orbits to loose their stability and give birth to further closed invariant curves with frequencies different from that of the parent periodic orbit in the state space. Depending on the relation of the frequencies of the new orbits with that of the parent orbit, the newly formed orbits may be periodic or quasi-periodic.

The memristive MLC circuit being a piecewise-smooth system with two discontinuity boundaries $\Sigma_{1,2}$ and $\Sigma_{2,3}$ defined by the zeros of two scalar functions $H_1(\mathbf{x}, \mu)$ and $H_2(\mathbf{x}, \mu)$, its state equations, refer Eq. (16), are given as a set of smooth ODEs,

$$\dot{\mathbf{x}}(t) = \begin{cases} F_2(\mathbf{x}, \mu), & H_1(\mathbf{x}, \mu) \geq 0 \ \& \ H_2(\mathbf{x}, \mu) < 0, \ x \in S_2, \\ F_{1,3}(\mathbf{x}, \mu), & H_1(\mathbf{x}, \mu) < 0 \ \& \ H_2(\mathbf{x}, \mu) \geq 0, \ x \in S_{1,3}, \end{cases} \quad (37)$$

where μ denotes the parameter dependence of the vector fields and the scalar functions. The vector fields F_i 's are

$$F_i(\mathbf{x}, \mu) = \begin{pmatrix} x_2 \\ -a_i x_2 + x_3 \\ -\beta x_2 - \beta x_3 + f \sin(\omega x_4) \\ 1 \end{pmatrix}, \ i = 1, 2, 3. \quad (38)$$

The variational equation for the system was set up by substituting Eq. (37) in Eq. (34), where $D_x F(\phi_t(\mathbf{x}_0, t_0), t)$ is given as

$$D_x F(\phi_t(\mathbf{x}_0, t_0), t) = \begin{pmatrix} 0 & 1 & 0 \\ 0 & W & 1 \\ 0 & -\beta & -\beta \end{pmatrix},$$

with $W = q(a_1 - a_2) - a_1$, $q \in [0, 1]$. The solution of this variational equation was obtained numerically. As this involves both $\phi_t(\mathbf{x}_0, t_0)$ and $\Phi_t(\mathbf{x}_0, t_0)$, the variational equation was appended to the original system to obtain the combined system

$$\begin{cases} \dot{\mathbf{x}} \\ \dot{\Phi} \end{cases} = \begin{cases} F_i(\mathbf{x}, t) \\ D_x F_i(\mathbf{x}, t)\Phi \end{cases}. \quad (39)$$

This combined system of equations was solved simultaneously by numerical integration for a time $T = \left(\frac{2\pi}{\omega}\right)$ assuming the initial conditions

$$\begin{cases} \mathbf{x}(t_0) \\ \Phi(t_0) \end{cases} = \begin{cases} \mathbf{x}_0 \\ I \end{cases}. \quad (40)$$

where I is an identity matrix.

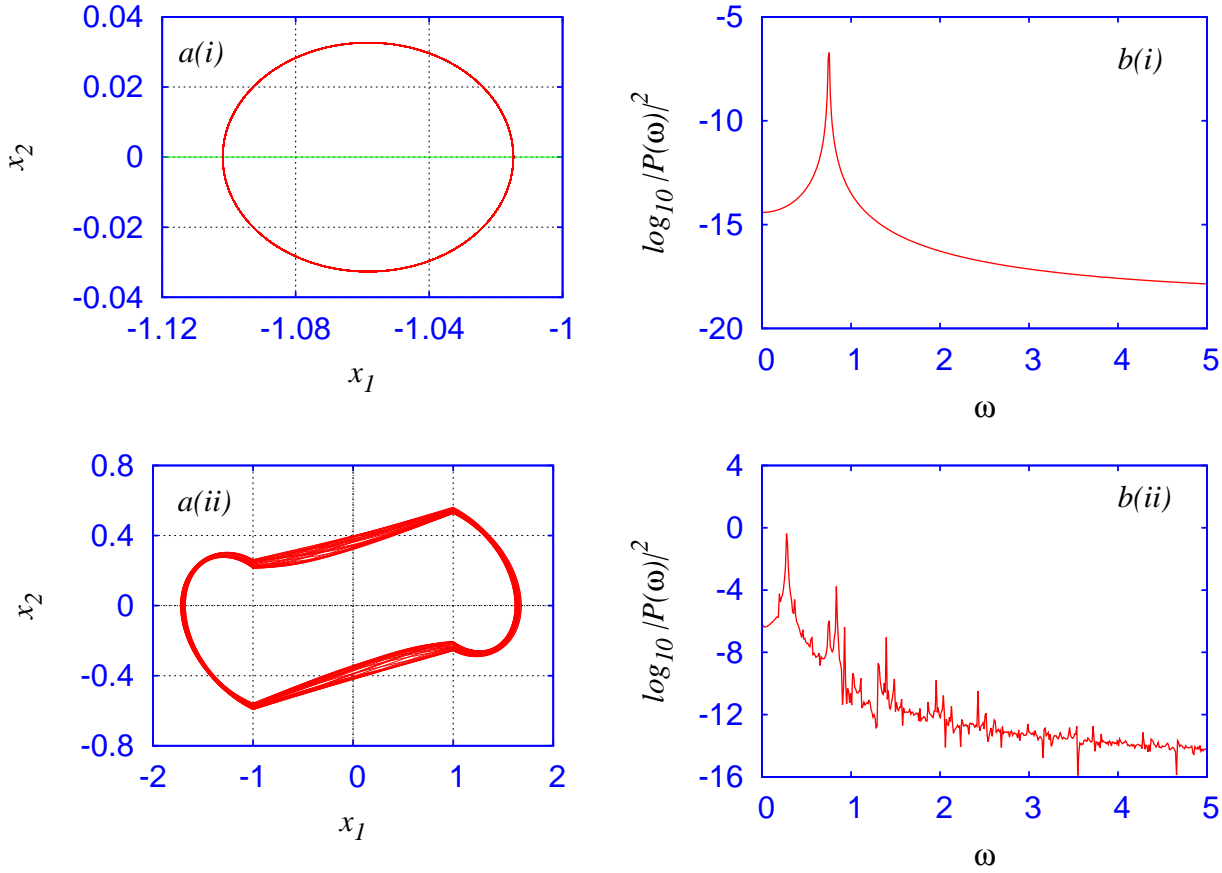


Fig. 13. Phase portraits a(i) and a(ii) and their corresponding power spectra b(i) and b(ii) for the memristive MLC circuit before and after a Neimark-Sacker bifurcation. The single peak at a frequency $\omega = 0.755310$ very close to the frequency of the external force and a peak power of $\log_{10}|P(\omega)|^2 = -6.714105$ of the power spectrum in b(i) represents that of the forced oscillations while the Dirac delta peaks of the power spectrum in b(ii) confirms the quasi-periodic behaviour.

The normalised circuit parameters are assumed to be the same as before with $a_{1,3} = -0.55$, $a_2 = -1.02$, with the normalised angular frequency of the external periodic forcing as $\omega_{ext} = 0.75$ and the amplitude of the external force as $f = 0.01$. The parameter β is assumed as the control parameter for the system and the auxiliary variable is set as $q = 0.5$. The eigenvalues of this generalised monodromy matrix so obtained, namely m_{q_i} 's, are also set valued $q \in [0, 1]$.

The variations of the Floquet multipliers as a function of the control parameter in the range $0.6 < \beta < 1.2$ for two different cases were investigated. Firstly the monodromy matrix was set up in a manner similar to that of a smooth system. Secondly the generalised monodromy matrix was constructed by applying the concept of Clarke's generalised differential. These variations are shown in Fig. 12 (a) and (b) respectively. As is expected from Floquet theory, one of the characteristic multipliers is always unity, that is $m_1 = m_{q_1} = 1$. In Fig. 12 (a) the other two characteristic multipliers are negative $m_{2,3} = < 0$. This tells that the periodic orbit arising due to forced oscillations is highly stable and hence no further bifurcations or any new attractors are possible for the entire range $0.6 < \beta < 1.2$ of the control parameter. Hence the usual Floquet theory does not predict any Neimark-Sacker Bifurcation in the memristive MLC circuit.

However in Fig. 12 (b) the set-valued characteristic multipliers $m_{q_{2,3}}$ cross the imaginary axis as a complex conjugate pair at a critical value of the control parameter $\beta_m = 0.9$. Above this critical value of β the real part of $m_{q_{2,3}}$ is negative while it crosses the zero axis at the critical value and becomes positive thereafter. This shows that for control parameter above the critical value, that is for $\beta > \beta_m$ the periodic

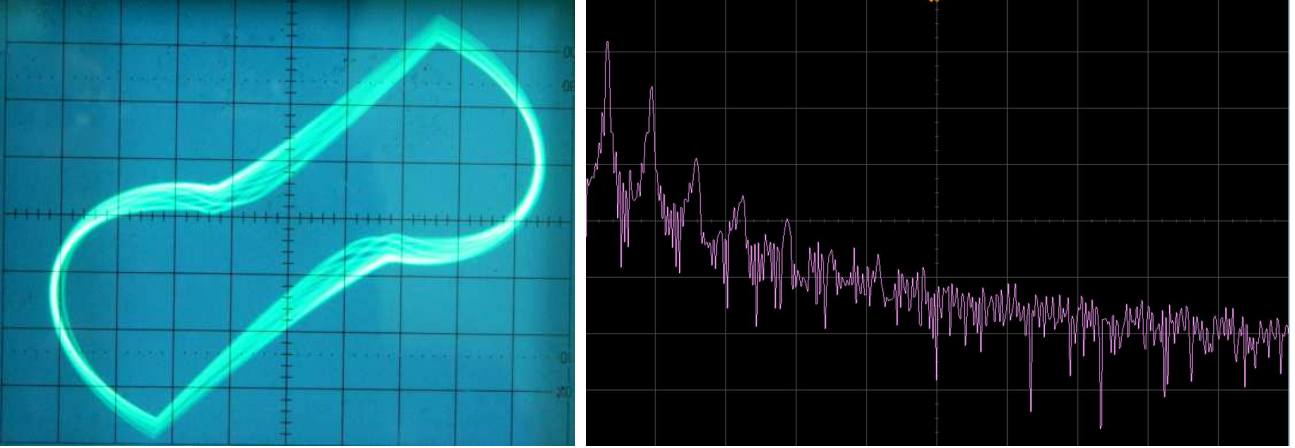


Fig. 14. Figure showing (a) the experimental phase portrait in the $(\phi - v_c)$ plane of the quasi-periodic motion arising due to discontinuous Neimark-Sacker bifurcation, corresponding to the numerical phase portrait in Fig. 13 a(ii). The experimental values of the circuit elements are $L = 300mH$, $C = 40nF$, amplitude $F = 380mV_{pp}$ (peak-to-peak voltage) and frequency $f = 1.972KHz$ for the externally applied force and (b) the power spectrum of the voltage across the capacitor v_c , corresponding to the numerical spectrum shown in Fig. 13 b(ii), depicting Dirac delta peaks, confirming the occurrence of quasi-periodic motion.

orbit is stable, while below it, the periodic orbit loses its stability giving birth to a newer periodic orbit as a result of *discontinuity induced Neimark-Sacker* bifurcation. The frequency of the new orbit may be different from that of the parent one. Further the memristor modulation causes once again the periodic orbit to become a n -frequency quasi-periodic attractor.

The stable periodic orbit due to forced oscillations is shown in the phase portrait in Fig. 13 a(i). Its corresponding power spectrum shown in Fig 13 b(i) contains just a single peak at a frequency $\omega = 0.755310$ very close to the frequency of the external force ($\omega_{ext} = 0.75$) and a peak power of $\log_{10}|P(\omega)|^2 = -6.714105$. Similarly the phase portrait in Fig. 13 a(ii) and the Dirac delta peaks in its corresponding power spectrum in Fig. 13 b(ii) show clearly the quasi-periodic nature of the attractor.

As in the case of Hopf Bifurcation, the experimental observation of the Neimark-Sacker Bifurcation was also obtained. For this, the parameters of the memristive part of the circuit as well as the inductance and capacitance values, namely $L = 300mH$ and $C = 40nF$ were retained as were fixed earlier for observing Hopf Bifurcation. However when the amplitude and frequency of the external force were increased, we observed Neimark-Sacker bifurcation taking place. The experimental phase portrait in the $(\phi - v_c)$ plane of the quasi-periodic motion when the amplitude of the external force $F = 380mV_{pp}$ with its frequency being $f = 1.972KHz$ and the power spectrum of the voltage v_c across the capacitor are shown in Fig. 14. These correspond well to the phase portrait in the $(x_1 - x_2)$ plane shown in Fig. 13 a(ii) and the power spectrum of the x_2 normalised variable shown in Fig. 13 b(ii) respectively.

8. Conclusion

In this paper we have considered the memristive Murali-Lakshmanan-Chua circuit as a non-smooth dynamical system and studied its peculiar behaviour arising due to the piecewise continuous nature of the memristor, its switching ability, time variation properties and modulation characteristic. We have done this by identifying and setting up switching manifolds, reformulating the system equations as a set of smooth ODEs and by construction of discontinuity mapping corrections such as the Poincaré Discontinuity Mapping and Zero Time Discontinuity Mapping corrections at these switching boundaries. The details of these discontinuity mapping corrections can be referred from our earlier work, [Ishaq & Lakshmanan, 2013]. We have found out the equilibrium points admitted by this system, evaluated their stability. The discontinuity induced bifurcations occurring at switching manifolds were analysed. We predicted using Clarke's generalised Jacobian theory the occurrence of discontinuous Hopf bifurcations in the unforced case and using proper modifications of the Floquet theory the existence of Neimark-Sacker bifurcations in the system in

the presence of the external forces. We have verified these with the help of numerical simulations as well as real hardware experiments. To the best of our knowledge it is for the first time that discontinuity induced Hopf and Neimark-Sacker bifurcations were identified and studied in a memristive piecewise continuous system.

9. References

Acknowledgments

This work has been supported by a NASI Platinum Jubilee Senior Scientist fellowship to M.L.

Appendix A

Piecewisessmooth Continuous Systems

A dynamical system may be defined as a deterministic mathematical prescription for evolving the state of a physical entity forward in time. If this time evolution arises as a smooth function of the arguments of the dynamical system, then it is termed as a *smooth dynamical system*. However if the time evolution of the dynamics of the system arises as a nonsmooth function of the arguments, then the dynamical system is termed as a *nonsmooth* or *piecewise smooth* system. The piecewise smooth systems are found to possess one or many discontinuity boundaries. The *discontinuity boundaries* are defined as the sets $\Sigma_{i,j}$ that separate the phase space of a piecewise smooth system into different regions [Nordmark, 1991]. They are also referred to in literature as *discontinuity sets* or *switching manifolds*. They are identified by the zeros of some scalar functions, say $H(\mathbf{x})$. If the piecewise smooth systems take on a continuous time evolution behaviour at the discontinuity boundaries, then the systems are called as *piecewise smooth continuous systems*.

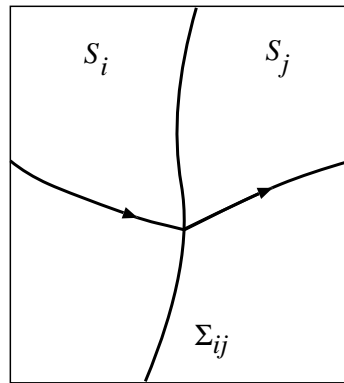


Fig. A.1. Schematic illustration of the trajectories of a piecewise-smooth flow crossing the switching manifold $\Sigma_{i,j}$ from the subspace S_i to S_j

Generally the piecewise smooth continuous systems are described by a finite set of continuous ODEs

$$\dot{\mathbf{x}} = F_i(\mathbf{x}, \mu), \quad \text{for } \mathbf{x} \in S_i \quad (\text{A.1})$$

where S_i 's are the subspaces of the phase space created by one or more *discontinuity boundaries* $\Sigma_{i,j}$'s as shown in Fig. A.1. Let us consider a piecewise-smooth system having a single discontinuity set $\Sigma_{1,2}$

identified by the zeros of the scalar function $H(\mathbf{x}, \mu)$, such that Eq. (A.1) can be explicitly written as

$$\dot{\mathbf{x}} = \begin{cases} F_1(\mathbf{x}, \mu), & \text{if } H(\mathbf{x}, \mu) < 0, \mathbf{x} \in S_1 \\ F_2(\mathbf{x}, \mu), & \text{if } H(\mathbf{x}, \mu) > 0, \mathbf{x} \in S_2 \end{cases} \quad (\text{A.2})$$

This system will have

- (1) a degree of smoothness *one* if $F_1(\mathbf{x}, \mu) \neq F_2(\mathbf{x}, \mu)$ at $\mathbf{x} \in \Sigma_{1,2}$.
- (2) a degree of smoothness *two* if $F_1(\mathbf{x}, \mu) = F_2(\mathbf{x}, \mu)$, but $\frac{\partial F_1}{\partial x} \neq \frac{\partial F_2}{\partial x}$ at $\mathbf{x} \in \Sigma_{1,2}$.
- (3) a degree of smoothness *three* if $F_1(\mathbf{x}, \mu) = F_2(\mathbf{x}, \mu)$ and $\frac{\partial F_1}{\partial x} = \frac{\partial F_2}{\partial x}$, but $\frac{\partial^2 F_1}{\partial x^2} \neq \frac{\partial^2 F_2}{\partial x^2}$ at $\mathbf{x} \in \Sigma_{1,2}$.

If the degree of smoothness of a piecewise-smooth continuous system is *one*, then the system is called a *Filippov System* [Filippov, 1964, 1988]. Filippov systems admit a complex type of behaviour called *sliding motion*. However if the degree of smoothness of the system is greater than or equal to *two*, then the system is called as a *Piecewise-smooth Continuous Flow* or simply a *Flow*. A large number of piecewise smooth continuous systems belong to either of these types. For example the familiar Chua's oscillator and the MLC oscillator, both for long considered as paradigmatic examples in the study of chaos, can behave either as a Filippov system or as a piecewise-smooth continuous flow under appropriate conditions. The discontinuity sets in the Chua and MLC oscillator arise because of the piecewise-linear nature of their nonlinear resistive element, namely the Chua's diode. However the chaotic dynamics exhibited by these systems is attributed to a sequence of smooth bifurcations. The presence of discontinuity boundaries in these systems seem to affect only the geometrical structure of the chaotic attractor, see [di Bernardo *et al.*, 2008].

Discontinuity Induced Bifurcation (DIB)

A discontinuity-induced bifurcation is said to occur at a particular parameter value if there exists an arbitrary small perturbation that causes the system to lose its piecewise-structural equivalence [di Bernardo *et al.*, 2008]. Different types of discontinuity-induced bifurcations (DIBs) are found to arise, such as border collision in maps, boundary equilibrium bifurcations, grazing bifurcations, sticking and sliding bifurcations and border intersection bifurcations in piecewise smooth continuous systems. These bifurcations are referred to in Russian and East European literature [Feigin, 1970, 1994] as *C-Bifurcations*. The Russian letter '*C*' pronounced as '*S*' stands for *sewing*, as one sews together two different trajectory segments on either side of the discontinuity boundary.

Equilibrium Points of a Piecewise Smooth Continuous System

A piecewise-smooth continuous flow will have two types of equilibrium points, namely (i) admissible equilibrium point and (ii) boundary equilibrium point. A point $x \in S$ is an *admissible equilibrium point* of Eq. (A.1), if

$$\begin{aligned} F_1(\mathbf{x}, \mu) &= 0, \\ H(\mathbf{x}, \mu) &:= \lambda_1 < 0. \end{aligned} \quad (\text{A.3})$$

or

$$\begin{aligned} F_2(\mathbf{x}, \mu) &= 0, \\ H(\mathbf{x}, \mu) &:= \lambda_2 < 0. \end{aligned} \quad (\text{A.4})$$

This admissible equilibrium point is also known as a *virtual equilibrium point*. A point $\hat{\mathbf{x}}$ is a *boundary equilibrium point* of Eq. (A.1), if

$$\begin{aligned} F_1(\hat{\mathbf{x}}, \mu) = 0, \quad \text{or} \quad F_2(\hat{\mathbf{x}}, \mu) = 0, \\ H(\hat{\mathbf{x}}, \mu) = 0. \end{aligned} \quad (\text{A.5})$$

Boundary Equilibrium Bifurcations (BEB)

The boundary equilibrium bifurcations are analogous to the border-collision bifurcations in maps. A piecewise-smooth system is said to undergo a boundary equilibrium bifurcation [di Bernardo *et al.*, 2008], at $\mu = \mu^*$ if there exists a point x^* such that for all values of $i = 1, 2, 3$:

$$\begin{aligned} F_i(\mathbf{x}^*, \mu^*) &= 0 \\ H_i(\mathbf{x}^*, \mu^*) &= 0 \\ \det(F_{i,\mathbf{x}}) &\neq 0 \\ P(\mathbf{x}^*, \mu^*) &\neq 0, \end{aligned} \tag{A.6}$$

where

$$P(\mathbf{x}^*, \mu^*) = H_{i,\mu}(\mathbf{x}^*, \mu^*) - H_{i,\mathbf{x}}(\mathbf{x}^*, \mu^*) \left[F_{i,x}^{-1} F_{i,\mu} \right] (\mathbf{x}^*, \mu^*). \tag{A.7}$$

Here the second subscripts denote the derivatives of the function with respect to the variables represented by those subscripts, namely

$$\begin{aligned} H_{i,x}(\mathbf{x}^*, \mu^*) &= \left. \frac{\partial H_i(\mathbf{x}, \mu)}{\partial x} \right|_{\mathbf{x}=\mathbf{x}^*, \mu=\mu^*} \\ H_{i,\mu}(\mathbf{x}^*, \mu^*) &= \left. \frac{\partial H_i(\mathbf{x}, \mu)}{\partial \mu} \right|_{\mathbf{x}=\mathbf{x}^*, \mu=\mu^*} \\ F_{i,x}(\mathbf{x}^*, \mu^*) &= \left. \frac{\partial F_i(\mathbf{x}, \mu)}{\partial x} \right|_{\mathbf{x}=\mathbf{x}^*, \mu=\mu^*} \\ F_{i,\mu}(\mathbf{x}^*, \mu^*) &= \left. \frac{\partial F_i(\mathbf{x}, \mu)}{\partial \mu} \right|_{\mathbf{x}=\mathbf{x}^*, \mu=\mu^*}. \end{aligned} \tag{A.8}$$

The first two equations give the defining conditions for a boundary equilibrium bifurcation to occur at \mathbf{x}^* for a parameter value $\mu = \mu^*$. The third equation ensures that \mathbf{x}^* is an *isolated hyperbolic* equilibrium point for the vector fields F_i 's. The final equation is a non-degeneracy condition with respect to the parameter μ , that the admissible branches of the equilibria cross the bifurcation point \mathbf{x}^* at $\mu = \mu^*$.

Linearising the system described by Eq. (A.2) about its boundary equilibrium point, $\mathbf{x} = 0$, $\mu = 0$, we have

$$\begin{aligned} N_1 \mathbf{x}^- + M_1 \mu &= 0, \\ C^T \mathbf{x}^- + D \mu &= \lambda^-, \end{aligned} \tag{A.9}$$

and

$$\begin{aligned} N_2 \mathbf{x}^+ + M_2 \mu &= N_1 \mathbf{x}^+ M_1 \mu + E \lambda^+ = 0, \\ C^T \mathbf{x}^+ + D \mu &= \lambda^+, \end{aligned} \tag{A.10}$$

where $N_1 = F_{1,x}$, $M_1 = F_{1,\mu}$, $C^T = H_x$, $D = H_\mu$ and $\mathbf{x}^+(\mu)$ and $\mathbf{x}^-(\mu)$ are the branches of the equilibria, before and after the crossing of the discontinuity boundaries at $\mu = \mu^*$ in the sub-regions S_1 and S_2 of the vector fields $F_1(\mathbf{x}, \mu)$ and $F_2(\mathbf{x}, \mu)$ respectively.

From the above relations, the conditions for the occurrence of boundary equilibrium bifurcations (BEBs) can be inferred.

Persistence

A persistence refers to the change of the nature of the equilibrium point from being admissible to virtual and vice versa upon crossing of the discontinuity boundary. This bifurcation is observed if the following conditions are satisfied

$$\det(N_1) \neq 0, \tag{A.11}$$

$$D - C^T N_1^{-1} M_1 \neq 0, \tag{A.11}$$

$$1 + C^T N_1^{-1} E > 0. \tag{A.12}$$

Non-smooth Fold

A non-smooth fold refers to the conversion collision of two branches of *admissible equilibria* upon intersection of the discontinuity boundary to two branches of *virtual equilibria* and vice versa. This bifurcation is observed if

$$\begin{aligned} \det(N_1) &\neq 0, \\ D - C^T N_1^{-1} M_1 &\neq 0, \end{aligned} \quad (\text{A.13})$$

$$1 + C^T N_1^{-1} E < 0. \quad (\text{A.14})$$

Appendix B

Clarke's Theory of generalised differentials and generalized Jacobians

Let us consider a smooth continuous function $f(x)$. Then the classical derivative of this function at any point x can be defined by the tangent line to the graph of $f(x)$ at that point x , namely

$$f'(x) = \frac{\partial f(x)}{\partial x} = \lim_{y \rightarrow x} \frac{f(y) - f(x)}{y - x}. \quad (\text{B.1})$$

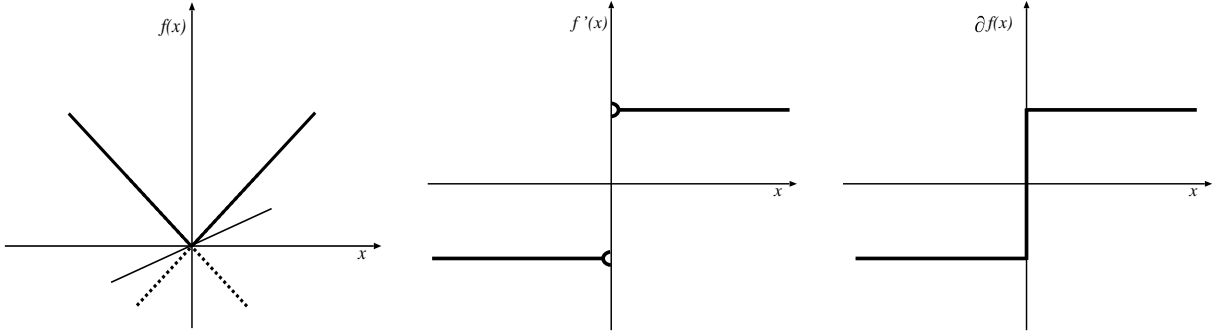


Fig. B.1. The geometrical representation of (a) the function $f(x) = |x|$, (b) its classical derivative $f'(x)$ and (c) the generalized derivative $\partial f(x)$.

If the function is piecewise continuous instead, having a non-smooth point at x , for example a kink as shown in Fig. (B.1), then the function $f(x)$ will not be absolutely differentiable at every point x . However such a function will possess at each point x , a left and a right derivative defined as, refer [Leine, 2006]

$$\begin{aligned} f'_-(x) &= \lim_{y \uparrow x} \frac{f(y) - f(x)}{y - x}, \\ f'_+(x) &= \lim_{y \downarrow x} \frac{f(y) - f(x)}{y - x}. \end{aligned} \quad (\text{B.2})$$

Then the generalized derivative of the function $f(x)$ at the non-smooth point x is declared as *any value* $f'_q(x)$ lying between its left and right derivatives [Clarke *et al.*, 1998]. Such an intermediate value can be expressed as a convex combination of the left and right derivatives,

$$f'_q(x) = (1 - q)f'_-(x) + qf'_+(x), \quad 0 \leq q \leq 1. \quad (\text{B.3})$$

Geometrically, a generalized derivative is the slope of any line drawn through the point $(x, f(x))$ and between the left and right tangent lines. The set of all generalized derivatives of f at x , or in general the convex hull of the extreme values of the derivative, is termed as the *generalized differential* of f at the point x ,

$$\begin{aligned} \partial f(x) &= \overline{\text{co}} \{f'_-(x), f'_+(x)\} \\ &= \{f'_q(x) | f'_q(x) = (1 - q)f'_-(x) + qf'_+(x), 0 \leq q \leq 1\}. \end{aligned} \quad (\text{B.4})$$

The generalized differential of Clarke at x is then the set of the slopes of all the lines included in the cone bounded by the left and right tangent lines and is a closed convex set. It is defined as

$$\partial f(x) = \bigcap_{\delta > 0} \overline{\text{co}} \{ \nabla f(y) | y \in x + B_\delta(0) \} \subset \mathcal{R}^{n \times m}, \quad (\text{B.5})$$

with the gradient

$$\nabla \mathbf{f}(\mathbf{x}) = \left(\frac{\partial \mathbf{f}(\mathbf{x})}{\partial \mathbf{x}} \right)^T \in \mathcal{R}^{n \times m}. \quad (\text{B.6})$$

The *generalized jacobian of Clarke* is then defined as the transpose of the generalized differential, namely

$$\mathbf{J}(\mathbf{x}) = (\partial \mathbf{f}(\mathbf{x}))^T \subset \mathcal{R}^{n \times m} \quad (\text{B.7})$$

Bifurcations refer to the qualitative changes in the structural behaviour of dynamical systems. In smooth dynamical systems which have smoothly varying vector fields, these bifurcations are associated with an eigenvalue or a pair of complex eigenvalues, passing through the imaginary axis under the variation of a control parameter. This automatically implies the dependency of the Jacobian matrices on the control parameters. However nonsmooth continuous systems possess discontinuity boundaries over which the vector fields are non-smooth. Due to this reason the classical Jacobian matrices cannot be obtained using the usual approach. It is in this context that people have applied the concept of Clarke's generalized differential to obtain the Jacobian matrix and its eigenvalues at the discontinuity boundaries.

Let us consider an autonomous non-smooth continuous system described by Eq. (A.2). Let x_μ be an equilibrium point of this system for some value of μ . This means that the Jacobian matrix which defines locally the vector field around the equilibrium point is single valued and is defined by.

$$J(x_\mu, \mu) = \begin{cases} J_-(\mathbf{x}_\mu, \mu) = \left. \frac{\partial F_1(\mathbf{x}, \mu)}{\partial x} \right|_{\mathbf{x}=\mathbf{x}_\mu}, & \mathbf{x}_\mu \in S_1 \\ J_+(\mathbf{x}_\mu, \mu) = \left. \frac{\partial F_2(\mathbf{x}, \mu)}{\partial x} \right|_{\mathbf{x}=\mathbf{x}_\mu}, & \mathbf{x}_\mu \in S_2. \end{cases} \quad (\text{B.8})$$

However the Jacobian matrices *jump* at the discontinuity boundary $\Sigma_{i,j}$. The *generalized Jacobian matrix* is therefore a convex combination of two matrices $J_-(\mathbf{x}, \mu)$ and $J_+(\mathbf{x}, \mu)$. It gives the set of all values which the *generalized Jacobian* can take on the discontinuity boundary $\Sigma_{i,j}$, namely

$$\begin{aligned} J(\mathbf{x}, \mu) &= \overline{\text{co}} \{ J_-(\mathbf{x}, \mu), J_+(\mathbf{x}, \mu) \} \\ &= \{ (1 - q)J_-(\mathbf{x}, \mu) + qJ_+(\mathbf{x}, \mu), \forall q \in [0, 1] \}. \end{aligned} \quad (\text{B.9})$$

Thus the generalized Jacobian can be visualised to give a unique path of eigenvalues during the *jump* as auxiliary variable q is varied from 0 to 1.

References

- Babitskii, V. I. [1978] *Theory of Vibroimpact Systems: Approximate Methods* (Nauka, Moscow).
- Bao, B. C., Liu, Z. & Xu, J. [2010] "Steady periodic memristor oscillator with transient chaotic behaviours," *Electron. Lett.* **46**, 237–238.
- Bo-Cheng, B., Zhong, L. & Jian-Ping, X. [2010] "Transient chaos in smooth memristor oscillator," *Chin. Phys. B* **19**, 030510.
- Buscarino, A., Fortuna, L., Frasca, M., Gambuzza, L. V. & Sciuto, G. [2012] "Memristive chaotic circuits based on cellular nonlinear networks," *Int. J. Bifurcation and Chaos* **22**, 1250070.
- Chua, L. [1971] "Memristor- the missing circuit element," *IEEE Trans. Circuit Th. CT-V.* **18**, 507–519.
- Chua, L., Desoer, C. A. & Kuh, E. S. [1987] *Linear and Nonlinear Circuits* (McGraw-Hill Book Company, Singapore).
- Chua, L. O. [2011] "Resistive switching memories are memristors," *Appl. Phys. A* **102**, 765–783.
- Chua, L. O. [2014] "If It's Pinched It's a Memristor," *Memristors and Memristive Systems* (Springer), pp. 17–31.

- Clarke, F. H., Ledyev, Y. S., Stern, R. J. & Wolenski, P. R. [1998] *Nonsmooth Analysis and Control Theory, in : Graduate Texts in Mathematics*, Vol. 178 (Springer, New York).
- Corinto, A., Fernando. Ascoli & Gilli, M. [2011] “Nonlinear dynamics of memristor oscillators,” *IEEE CAS.-I* **58**, 1323–1336.
- di Bernado, M., Budd, C., Champneys, A. & Kowalczyk, P. [2008] *Piecewise-smooth Dynamical Systems: Theory and Applications* (Springer-Verlag, London).
- di Bernardo, M., Budd, C. J., Champneys, A. R., Kowalczyk, P., Nordmark, A. B., Olivar, G. T. & Piiroinen, P. [2008] “Bifurcations in nonsmooth dynamical systems,” *SIAM Review*. **50**, 629–701.
- di Bernardo, M., Garofalo, F., Ianneli, L. & Vasca, F. [2002] “Bifurcations in piecewise-smooth feedback systems,” *International Journal of Control*. **75**, 1243–1259.
- Feigin, M. [1970] “Doubling of the oscillation period with C-bifurcations in piecewise continuous systems,” *Journal of Applied Mathematics and Mechanics* **34**, 861–869.
- Feigin, M. [1994] *Forced Oscillations in Systems with Discontinuous Nonlinearities* (Nauka, Moscow).
- Filippov, A. [1964] “Differential equations with discontinuous righthand-side,” *American Mathematical Society Translations, Series 2* **42**, 199–231.
- Filippov, A. [1988] *Differential Equations with Discontinuous Righthand Sides, Mathematics and its Applications* (Kluwer Academic Publishers, Dordrecht).
- Fu, S., Lu, Q. & Meng, X. [2015] “New discontinuity induced bifurcations in Chua’s circuit,” *Int. J. Bifurcation and Chaos*. **25**, 1550090:1–11.
- Galvanaetto, U. [1997] “Bifurcations and chaos in a four-dimensional mechanical system with dry friction,” *Journal of Sound and Vibrations* **204**, 690–695.
- Galvanaetto, U. [2001] “Some discontinuous bifurcations in a two block stick-slip system,” *Journal of Sound and Vibrations* **284**, 653–669.
- Galvanaetto, U. & Bishop, S. R. [1998] “Computational techniques for nonlinear dynamics in multiple friction oscillators,” *Computer Methods in Applied Mechanics and Engineering* **163**, 373–382.
- Ishaq, A. A. & Lakshmanan, M. [2013] “Nonsmooth bifurcations, transient hyperchaos and hyperchaotic beats in a memristive Murali-Lakshmanan-Chua circuit,” *Int. J. Bifurcation and Chaos* **23**, 1350098 (28 pages).
- Ishaq Ahamed, A., Srinivasan, K., Murali, K. & Lakshmanan, M. [2011] “Observation of chaotic beats in a driven memristive Chua’s circuit,” *Int. J. Bifurcation and Chaos*. **21**, 737–757.
- Itoh, M. & Chua, L. O. [2008] “Memristor oscillators,” *Int. J. Bifurcation and Chaos*. **18**, 3183–3206.
- Iu, H. H. C., Yu, D. S., Fitch, A. L., Sreeram, V. & Chen, H. [2011] “Controlling chaos in a memristor based circuit using a twin-T notch filter,” *IEEE CAS.-I* **58**, 1337–1344.
- Leine, R. I. [2006] “Bifurcations of equilibria in non-smooth continuous systems,” *Physica D*. **223**, 121–137.
- Leine, R. I. & Campen, D. H. [2002] “Discontinuous fold bifurcations in mechanical systems,” *Archive of Applied Mechanics* **72**, 138–146.
- Leine, R. I. & Campen, D. H. [2006] “Bifurcation phenomena in non-smooth dynamical systems,” *European J. Mech. A* **25**, 595–616.
- Leine, R. I., Campen, D. H. & van de Vrande, B. L. [2000] “Discontinuous nonlinear discontinuous systems,” *Nonlinear Dynamics* **23**, 105–164.
- Leine, R. I. & Nijmeijer, H. [2004] *Dynamics and Bifurcations in Non-smooth Mechanical Systems* (Springer-Verlag, Berlin).
- Messias, M., Nespoli, C. & Botta, V. [2010] “Hopf bifurcation from lines of equilibria without parameters in memristor oscillators,” *Int. J. Bifurcation and Chaos* **20**, 437–450.
- Muthuswamy, B. [2009] “Memristor based chaotic circuits,” Tech. Rep. UCB/EECS- 2009-6, Berkely University, Murray Hill, New Jersey, <http://www.eecs.berkeley.edu/Pubs/TechRpts/2009/EECS-2009-6.html>.
- Muthuswamy, B. [2010] “Implementing memristor based chaotic circuits,” *Int. J. Bifurcation and Chaos* **20**, 1335–1350.
- Muthuswamy, B. & Chua, L. O. [2010] “Simplest chaotic circuit,” *Int. J. Bifurcation and Chaos* **20**, 1567–1580.
- Muthuswamy, B. & Kokate, P. [2009] “Memristor based chaotic circuits,” *IETE Tech. Rev.* **26**, 417–429.

- Nordmark, A. B. [1991] “Non-periodic motion caused by grazing incidence in impact oscillators,” *Journal of Sound and Vibration* **2**, 279–297.
- Parker, T. S. & Chua, L. O. [1984] *Practical Numerical Algorithms for Chaotic Systems* (Springer-Verlag, New York).
- Petráš, I. [2010] “Fractional-order memristor-based Chua’s circuit,” *IEEE CAS*. **57**, 975–979.
- Strutkov, D., Snider, G., Stewart, D. & Williams, R. [2008] “The missing memristor found,” *Nature* **453**, 80–83.
- Tour, J. M. & He, T. [2008] “The fourth element,” *Nature* **453**, 42.
- Zhang, Z. & Bi, Q. [2012] “Bifurcation in a piecewise-linear circuit with switching boundaries,” *Int. J. Bifurcation and Chaos*. **22**, 1250034:1–18.